Escola Tècnica Superior d'Enginyeries
Industrial i Aeronàutica de Terrassa
UNIVERSITAT POLITÈCNICA DE CATALUNYA

Titulació:

GRAU EN ENGINYERIA EN VEHICLES AEROESPACIALS

Alumne:

ELOI MIRAMBELL MASRAMON

Títol del TFG:

EXPERIMENTAL STUDY OF FLOW THROUGH A SAVONIUS WIND TURBINE

Director del TFG:

PEDRO JAVIER GÁMEZ MONTERO

Co-director del TFG:

ROBERTO CASTILLA LÓPEZ

Tutor:

DANIEL GARCÍA ALMIÑANA

Convocatòria de lliurament del TFG:

JUNY DE 2015

Contingut d'aquest volum:

DOCUMENT 1.-MEMÒRIA

ETSEIAT

Experimental study of flow through a Savonius wind turbine

- REPORT -

Eloi Mirambell Masramon

Director: Pedro Javier Gámez Montero

Co-Director: Roberto Castilla López

Tutor: Daniel García Almiñana

Grau en Enginyeria en Vehicles Aeroespacials

June 12, 2015

Acknowledgements

First of all, I am very grateful for support and help provided by the director of this TFG, Pedro Javier Gámez Montero, and co-director, Roberto Castilla López, during the whole period of time this project has been done. Especially for their tips and guiding me in order to achieve the goals defined at the beginning of this study.

I would like to thank Dr. Gustavo Raush for his recommendations and explanations about wind tunnel and wind balance performances. I too wish to thank Dra. Mercedes Garcia Vilchez for allowing me to participate in one of her practical sessions in the laboratory of Fluid Mechanics Department.

I would like to express my gratitude to the technicians Jaume Bonastre and Justo Zoyo for their technical contributions to this project. Especially for their help in the 3D printing and in the usage of other machines placed in the laboratory facilities, without them this project had not been possible.

Finally, I would like to extend my gratitude to my colleague Pere Antoni Martorell, whose companionship has helped me in the development of this experimental study.

Contents

List of Figures

List of Tables

Nomenclature

H	height of the rotor [mm]	ϑ	rotor angular position [°]
D	diameter of the rotor [mm]	ρ	air density [kg/m^3]
D_f	diameter of the end plate [mm]	ρ_{man}	manometer alcohol density [kg/m^3]
ω	angular velocity of the rotor [rad/s]	l_0	manometer initial length [mm]
A_s	swept area of the rotor	l	alcohol column length [mm]
AR	aspect ratio of rotor	g	gravity [m/s^2]
R	radius of rotor [m]	$Temp$	laboratory temperature [ºC]
U	tip speed (ω·R)[m/s]	L	lift force [N]
V	wind velocity [m/s]	D	drag force [N]
N	rotational speed of rotor [RPM]	T	torque [Nm]
λ	tip speed ratio (U/V)	C_L	lift coefficient
e	overlap distance [mm]	C_D	drag coefficient
d_{shaft}	diameter of the shaft [mm]	C_P	power coefficient
d	diameter of blade [mm]	C_T	torque coefficient
β	overlap ratio	C_{Ts}	static torque coefficient
α	twist angle [°]	Re	Reynolds number
ψ	blade arc angle [°]	v	kinematic viscosity [m^2/s]
γ	manometer inclination angle [°]		

Chapter 1

1. Approach of the problem

1.1. Aim of the project

One of the main objectives of the present study is to design an own Savonius wind rotor based on previous experimental studies.

Another main objective is to carry out an experimental investigation in a wind tunnel to determine the aerodynamic behavior of air flow over the fixed Savonius wind turbine designed and obtain lift and drag coefficients.

A secondary objective is to obtain static torque coefficients of the wind turbine designed in order to analyze its starting torque characteristics.

1.2. Scope of the project

- Exhaustive bibliography research
- Theoretical and geometrical study of Savonius wind turbines
- Selection and design of the Savonius features
- 3D modeling of the Savonius rotor designed
- 3D printing of the Savonius rotor modeled
- Finishing process of the rotor printed
- Prepare the necessary equipment and the necessary material so as to carry out the experimental studies
- Development of the experiments and description of the procedure followed
- Analysis of the results obtained and post-treatment. Comparison with numerical and theoretical results.
- Determination of conclusions of the project and possible future works
- Writing all the necessary documents

The documents which are going to be written are the present report and 3 annexes. Annex I contains all the geometrical measures of Savonius wind turbine designed, Annex II contains the full tables and plots of results obtained in all experiments and, Annex III which contains the budget of this project.

1.3. Basic requirements of the project

1. 3D CAD software is necessary to make the appropriate 3D Savonius rotor model for the experimental study. Also the CAD software is able to provide the suitable file format for the 3D printer.

2. 3D printer must be used to print the 3D Savonius rotor model so as to obtain the rotor physically and allow working with it. Also, the printer must give the final rotor with an acceptable quality and high accuracy due to the high geometrical complexity of the model.

3. Wind tunnel is needed in order to carry out the experimental study. The wind tunnel must be operative and must incorporate an adequate test bench in order to set the Savonius rotor modeled.

4. Torque and force sensor are needed so as to compute the necessary data of the experimental tests. The sensors must provide the results with a suitable accuracy and with an admissible error. As a force sensor is going to be used an aerodynamic wind balance situated in the test bench of the wind tunnel.

5. Post-processing and data acquisition programs must give the appropriate tools in order to get the necessary treatment of the results. The post-processing programs also must be able to provide the required features so as to compare and verify the results obtained.

1.4. Justification of the project

This study is going to be carried out due to the great importance that the renewable energies are taking nowadays around the world. The usage of clean energy sources is being very popular because of the need of the human society to find inexhaustible energy resources. Then it is necessary to study all the possible renewable energies so as to get the maximum performance of each.

In this case it is going to be studied a Savonius wind turbine, which as its name indicates, is related to the wind energy. This kind of rotor has been already studied by many researchers in order to find the most efficient geometry and, hence, extract the maximum power of the wind. What this means is that this project is not going to discover new significant information about this topic. Then the purpose of the present project, apart from the aims mentioned at the beginning of this charter, is to obtain valid results which can be verified with the ones presented in the researches that have been already done.

However, almost all the studies carried out have been studying the torque and power that the Savonius rotor can give, clearly for energy purposes. In the other hand, only a few studies have studied the aerodynamic behavior and the aerodynamic forces produced by an air flow over the rotor. Therefore, a need of studying the aerodynamic performance of a Savonius wind turbine appears.

It also has to be said that the majority of studies which have been already done are relatively old. Then, with the help of the improved facilities and sensors that are going to be used in the Fluid Mechanics laboratory for this experimental study, it will be possible to extract more accurate measurements and in a faster way. In addition, the post-processing can be more extensive due to the many post-processing programs that currently exist for treating results.

In order to carry out the experimental study of the present project, a Savonius rotor is going to be designed based on all the researches already made, trying to achieve the most efficient geometry according to the restrictions of space fixed by the test bench of the wind tunnel. Then, apart from the aerodynamic analysis, a static torque study is wanted to be carried out so as to analyze the starting performance of the rotor designed so that compare it with other rotors of the bibliography.

In addition, this project is going to be useful to know the compatibility of the Fluid Mechanics laboratory to carry out a complete study of a wind turbine. Moreover, as a 3D printer is going to be used to build the Savonius rotor, this study will be able to check the resistance of a 3D printed body for doing experimental tests and being mechanized.

To sum up, considering the set of ideas that must be developed, it is clear that the experimental part will be essential in the development process of the project.

1.5. Background and state of the art

The renewable energy resources are becoming very important in recent years due to the environmental pollution and rising energy demand of our society. There are different options of renewable energy sources such as solar, hydroelectric and wind among others. The wind stands out because is a cheap and clean energy source that has huge potential in the world. During the last years a lot of wind turbines have been studied and developed so as to maximize the power of these machines.

Wind turbines can be classified in two general groups, the vertical axis wind turbine (VAWT) and horizontal axis wind turbine (HAWT).

Savonius wind rotor belongs to the vertical axis group. It was patented by the Finnish engineer Sigurd Savonius in 1929 and its main drawback is that has lower performance than other conventional wind rotors, but even so, it has some advantages over the others. The main ones are that these rotors are usually simple and hardy in structure and tend to be cheaper, they also have good starting characteristics, relatively low operating speeds and they are independent of wind direction.

As it has been said before, the Savonius rotor is a wind turbine that has been already studied for many scientists around the world. In general, all the investigations researched were studies of geometrical features of a Savonius rotor. In other words, they investigated which was the most efficient geometry in order to extract the most power of a Savonius.

The most useful conclusions of each of these studies analyzed have been summarized in a huge mental map shown in the Figure 1. It has to be said that this kind of diagram is very useful because allows to organize a lot of information in a very tidy way.

The schematized information in the mental map is widely explained in the chapter 2, specifically in the first section named "*Theoretical and Geometrical study*" which is the continuation of state of the art but in a more extensively way.

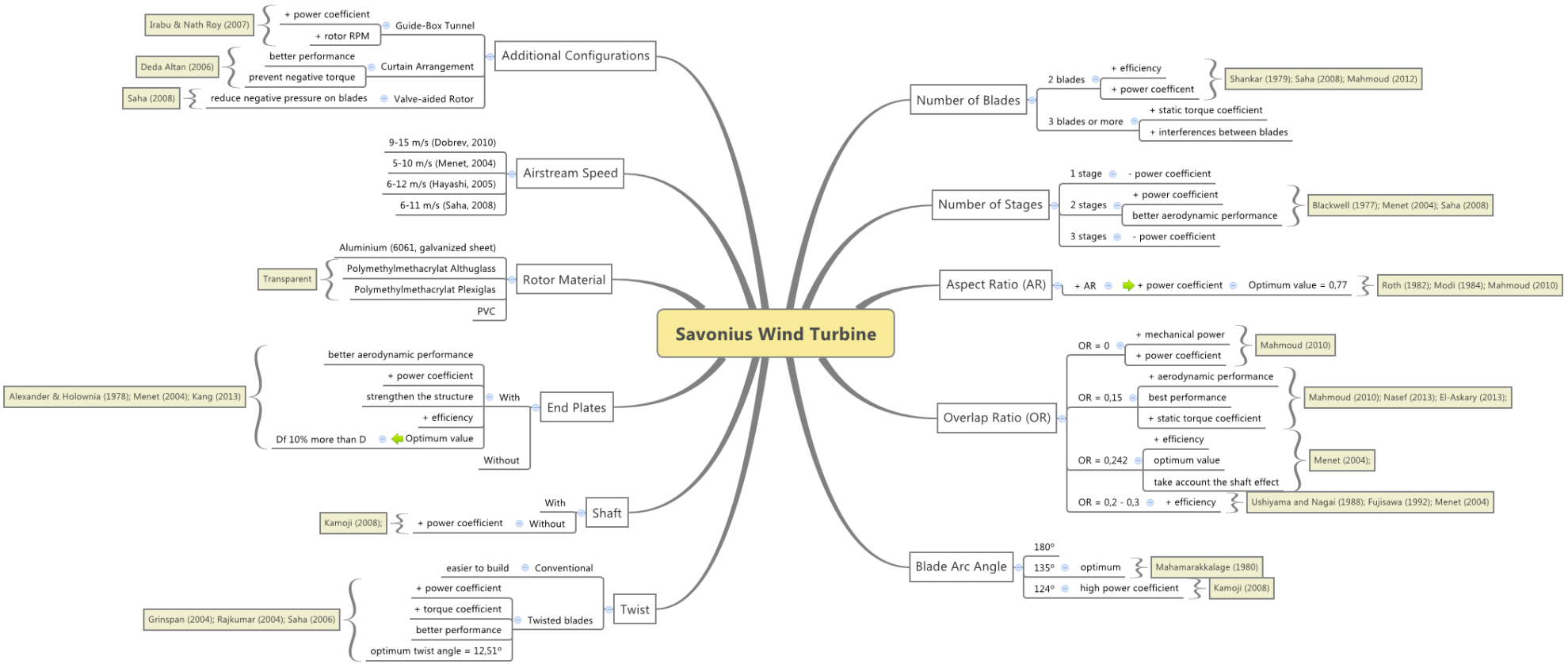

Figure 1 Mental map of state of the art of Savonius wind turbines

Chapter 2

2. Alternatives and solutions

2.1. Theoretical and Geometrical study

The conventional Savonius wind rotor is constructed simply of two vertical half cylinders and two end plates as it is shown in the Figure 2. But there are many variations of the conventional model rotor, such as number of blades, number of stages and twist among others.

Figure 2 Schematic of a Savonius rotor geometry [1]

As it has been said previously, the performance of this rotor has been studied by many researchers until nowadays in order to determine the optimum design. It has been carried out a good deal of theoretical, experimental and simulation studies so as to understand better the effect of each geometrical parameter of the rotor on its behavior.

In the Figure 3 it is possible to see how a Savonius wind turbine works.

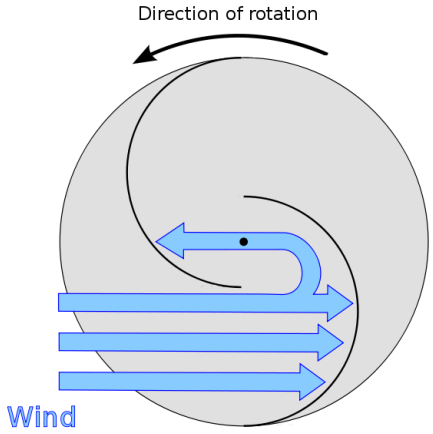

Figure 3 Performance of a Savonius wind turbine [2]

Ii is noted that the overlap distance that exists between the two blades allows the wind to go from one blade to the other. The wind strikes on the primary blade while it also pushes the secondary one favoring the rotation of the rotor. In this way, the overlap distance is one of the most interesting features of a Savonius wind turbine because it reduces the negative torque against the rotation of the rotor.

Therefore, in order to design the optimum Savonius rotor for the experimental study that is going to be carried out, a huge search of previous studies has been done and the following conclusions can be presented.

2.1.1. Number of blades

The effect of number of blades of the rotor has been investigated in many researches. All the results, according to Menet [3], Saha et al. [4] and Mahmoud et al. [5], concluded that a two bladed rotor gives higher efficiency and higher power coefficient than a three bladed rotor as it can be seen in the Figure 4, because when the number of blades increases the interferences of the air with blades increases too and, as a result, the angular speed of the rotor decreases.

In the Figure 4 it is also possible to see that the maximum power coefficient is produced when the tip speed ratio [λ] is about 0.6, independently from number of blades.

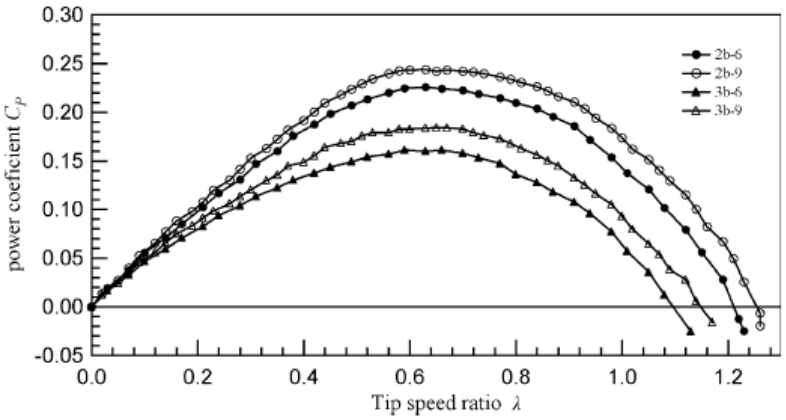

Figure 4 Power coefficients vs. tip speed ratio of the rotors for two and three blades and wind velocities V = 6 and 9 m/s [6]

However, a Savonius rotor designed with three blades (120º between each blade) generates favorable static torque characteristics at any phase angle whereas a two bladed rotor has angular positions where generates negative static torque. Although this, a two bladed rotor has a higher maximum static torque coefficient as it is shown in the Figure 5.

In addition, as it can be seen in the Figure 5, in the case of the rotor with two blades the maximum static torque coefficient is clearly produced in blade phase angle of 30° and 210° approximately, as Savonius rotor is symmetric and it has two periods of 180°. On the other hand, in the case of three blades three periods of 120° can be observed and the maximum is not as clear.

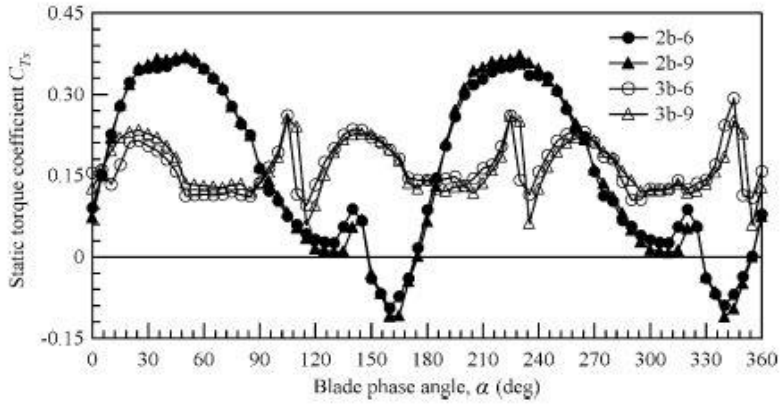

Figure 5 Static torque coefficient vs. phase angle for two and three blades rotor and wind velocities V = 6 and 9 m/s [6]

2.1.2. Number of stages

Another interesting parameter of Savonius rotors is the number of stages. Number of stages is the number of Savonius rotors that form the general structure of rotor system, generally one above the other as it is shown in the Figure 6.

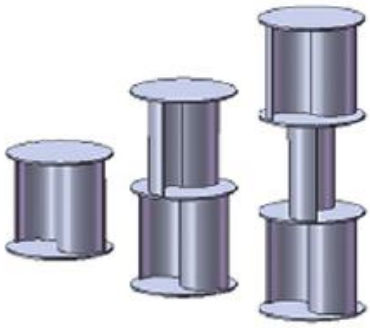

Figure 6 Models of single-, two- and three-stage rotor systems [7]

In most researches it has been studied the effect of a single, two and three stages rotors so as to get the optimum efficiency. Experiments concluded that the best number of stages for a Savonius turbine is clearly two according to Saha et al. [4], Mahmoud et al. [5] and Nasef et al. [8], because this configuration gives higher power coefficients above the others as it can be seen in the Figure 7. Moreover, it also shows better aerodynamic performance.

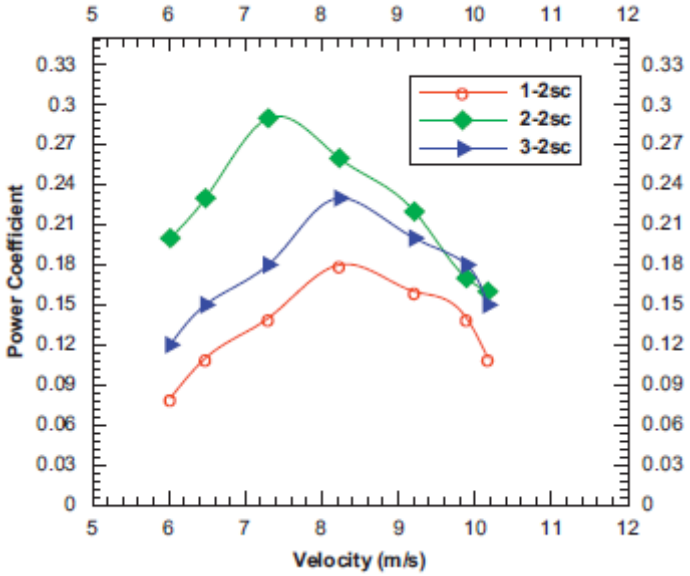

Figure 7 Power coefficient vs. wind velocity for two-bladed rotor system with different stages (sc=semicircular blades) [4]

2.1.3. Aspect ratio

The aspect ratio [AR] is a geometric parameter that is very interesting due to its relation with the rotor performance. It is defined as the ratio between rotor height and rotor diameter. A clear representation is shown in the Figure 8 where Savonius rotors with different aspect ratios are shown.

Figure 8 Savonius rotors with different aspect ratios [7]

The height of the rotor [H] is considered equal to the height of its blades and the diameter of the rotor [D] is the diameter of the circumference that rotor blades form when rotating.

Many researchers, like Alexander and Holownia [9] and Sivasegaram [10], deduced that there is an increase in power coefficient with the rise in aspect ratio. But the most interesting thing is that most researchers have concluded an optimum value of *AR* that gives the highest performance. This value is 0.77 according to Mahamarakkalage [11], Roth [12], and Modi et al. [13].

2.1.4. Overlap ratio

Another important parameter which affects the performance of a Savonius rotor is the overlap ratio [β]. It is defined as the ratio between the overlap distance [e] and the diameter of blades [d]. If rotor contains a shaft, then it is necessary to take into account the diameter of the corresponding shaft [d_{shaft}] versus the overlap distance. A representation of geometric parameters described is shown in the Figure 9.

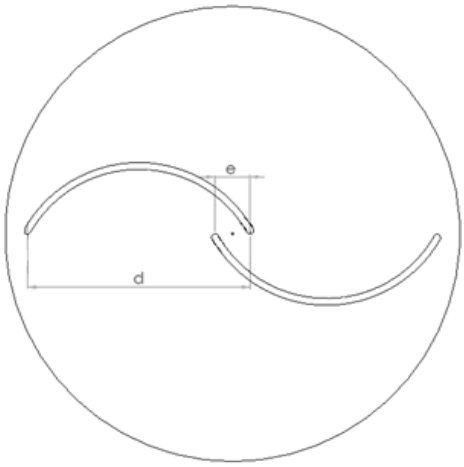

Figure 9 Representation of the overlap distance [e] and the blade diameter [d] in a two-bladed Savonius rotor

In this case it exists a disagreement about which is the effect of this geometric ratio. Mahmoud et al. [5] concluded that a rotor without overlap gives higher mechanical power than rotors with it as it is presented in the Figure 10.

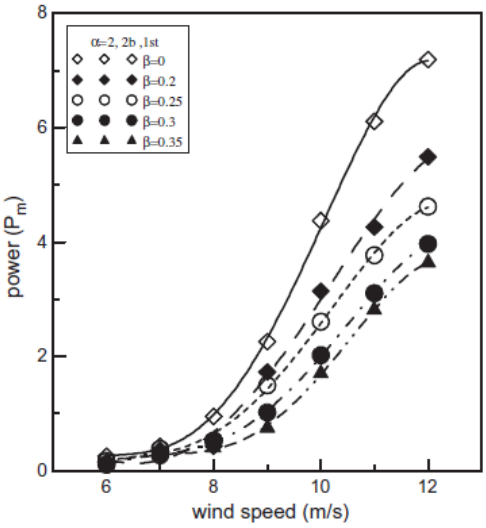

Figure 10 Mechanical power vs. wind speed for different overlap ratios [β] (α=AR, 1st=single stage, 2b=two blades) [5]

Others, like Nasef et al. [8] and Alexander and Holownia [9], said that increasing rotor overlap ratio increases the rotor efficiency and static torque coefficients, specially of the returning blade, and also that the best performance is the one which overlap ratio is equal to 0.15.

Finally there are the researchers Ushiyama and Nagai [14] and Fujisawa [15] who said that the value of overlap ratio that gives the best efficiencies is found between 0.2 and 0.3. Also, Menet [3] concluded that the optimum value of overlap ratio is 0.242, as it can

be seen in the Figure 11, which takes into account the blocking effect introduced by the shaft.

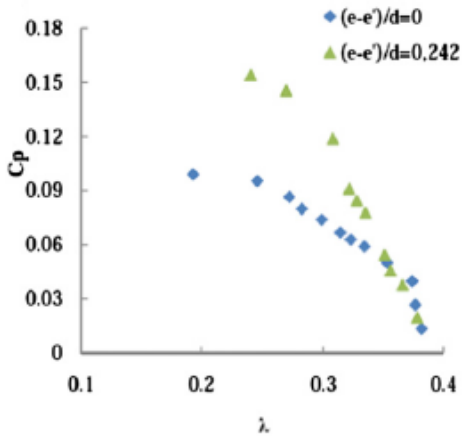

Figure 11 Variation of the power coefficient vs. tip speed ratio for two different overlap ratios [β] at constant Reynolds. Where *e* is the overlap distance, *e'* the shaft diameter and *d* the blades diameter [16]

2.1.5. Twist

A twisted Savonius rotor usually has two blades, each blade can be defined as a curve generated by a marker moving vertically at a constant velocity on a rotating cylinder at a constant angular velocity. The blade retains its cross-section from the bottom (0º) to the top (twist angle [α]). An example of a twisted rotor is shown in the Figure 12.

Figure 12 Savonius wind rotor with twisted blades [17]

The effect of twisted blades is clearly positive for a Savonius rotor. It has been proved that an helical rotor gives higher value of both power and torque coefficients, hence it develops better performance as compared to the conventional semicircular blade geometry according to Saha et al. [4] and Damak et al. [16].

It has been usually carried out researches with 180º twisted blades, but a series of investigations carried out by Grinspan [18] and Saha and Rajkumar [19] shown that the optimum twisted blades are the ones which are manufactured with a twist angle of 12.51°. The Figure 13 illustrates the power coefficient gain between a two bladed

conventional Savonius rotor versus a twisted one (twist [α] = 12.5°) for different stages. In the Figure 13 it is also noted that, as it has been said previously, the rotor with two stages gives higher power coefficients than rotors with one and three stages.

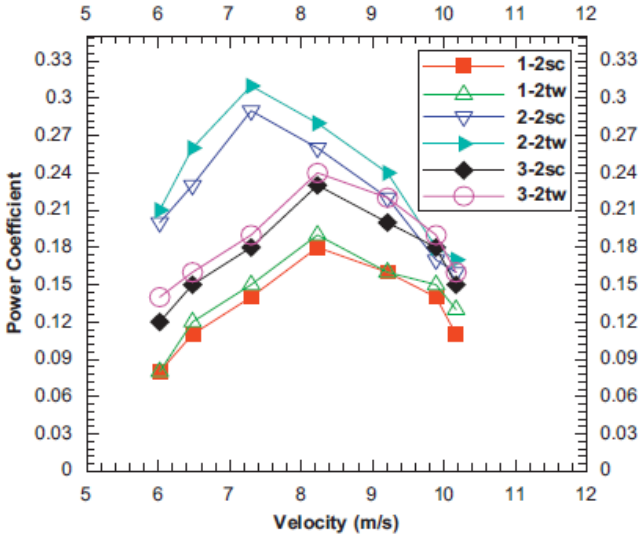

Figure 13 Variation of power coefficient vs. wind velocity for a two-bladed Savonius rotor. First number of the legend means number of stages, the second one is the number of blades (always 2), and then sc=semicircular (α=0°) and tw=twisted (α=12.5°) [4]

2.1.6. Blade arc angle

Blade arc angle [ψ] is a geometric parameter that describes the angular curvature of the cross-section of blade. Some researches have been done in the recent years in order to obtain the optimum value of this parameter, but the results obtained show discrepancy about what is the best curvature. A schematic representation of this geometrical parameter is shown in the Figure 14.

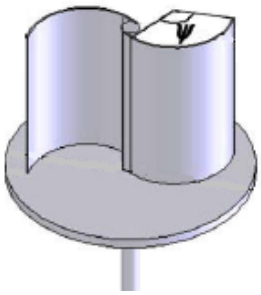

Figure 14 Blade arc angle parameter of Savonius rotor with shaft [20]

Kamoji et al. [20] said that a rotor with a blade arc angle of 124° is having the higher power coefficient compared to rotors with other blade arc angles, and other researchers

like Mahamarakkalage [11] concluded that the optimum value of blade arc angle is equal to 135°. Hence the results about this geometrical parameter are a bit confusing.

Figure 15 shows the experimental results obtained by rotors with different blade arc angles at fixed Reynolds number. It can be seen that the results are quite similar between different curvatures.

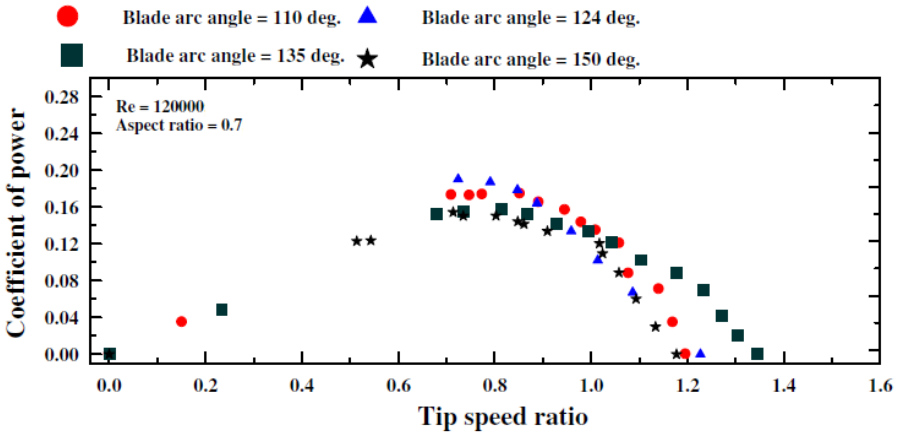

Figure 15 Effect of blade arc angle on the power coefficient at a Reynolds number of 120000 [20]

2.1.7. Shaft

The shaft is not an essential element for a Savonius wind turbine, but the main doubt is if the rotor is more efficient with or without it as it is shown in the Figure 16. The results obtained by Kamoji et al. [20] are clear because they show that a rotor without shaft has better performance and gives higher power coefficients. Although this conclusion, most times the shaft has to be used for structural and assembly reasons.

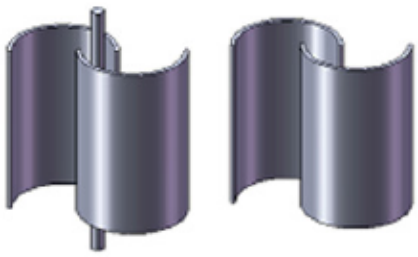

Figure 16 Interference of shaft [7]

2.1.8. End plates

The same occurs with end plates, two structural elements located at the extremes of the rotor. Some examples of end plates with different sizes are shown in the Figure 17.

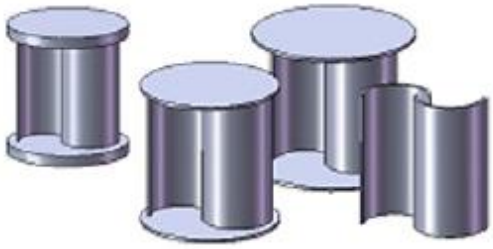

Figure 17 Example of different end plates

It can be seen that there are rotors even without end plates. Hence it is necessary to know if these elements improve or worsen the rotor performance. In this case the results are very clear, the researches of Menet [3], Mahmoud et al. [5], and Alexander and Holownia [9] show that end plates improve the aerodynamic performance and the efficiency of the rotor, hence power coefficients obtained are higher as it can be noted in the Figure 18. Moreover, according to Kang et al. [17], end plates have also a structural purpose because they strengthen the rotor structure.

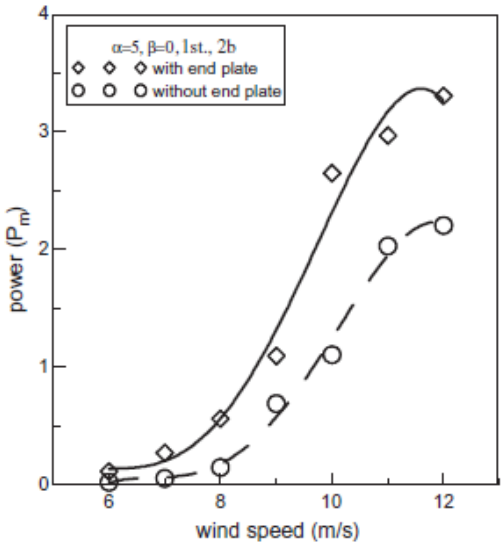

Figure 18 Mechanical power vs. wind speed for rotors with and without end plates (α=AR, 1st=single stage, 2b=two blades) [5]

Investigations of Menet [3] concluded that the optimum value for the diameter of the end plates [D_f] is around 10% greater than the rotor diameter [D].

2.1.9. Additional configurations

Some researchers studied and analyzed some extra devices or accessories so as to improve the performance of Savonius wind turbines.

2.1.9.1. Guide Box Tunnel

The purpose of the guide-box tunnel (GBT), according to Irabu and Roy [6], is to increase the rotational speed and the output power of the rotor in a range of low wind velocity. GBT is a strong structure which has two movable walls or gates and it has to adjust the inlet wind power by opening-shutting the inlet and the exit as it is shown in the Figure 19.

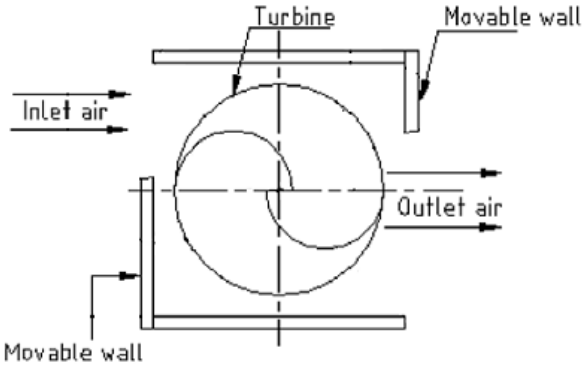

Figure 19 Schematic view of experimental rotor with GBT [6]

It was concluded that the rotation speed of the rotor depends on the area ratio of the inlet and outlet of GBT, then the maximum rotation speed was obtained in the range of area ratio from 0.3 to 0.7. In addition, using the GBT the maximum output power coefficient for the rotor is higher compared with the same rotor without GBT as it can be seen in the Figure 20.

It also can be observed that all the curves in Figure 20 have the maximum power coefficient in the tip speed ratio of 0.6 approximately, as it has been seen before at the beginning of this chapter.

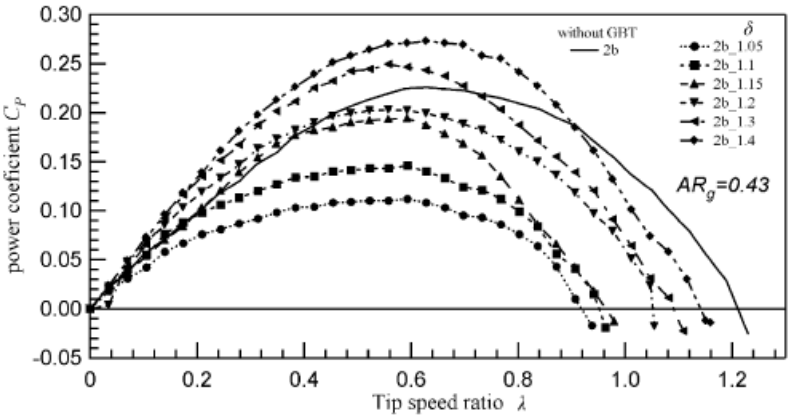

Figure 20 Power coefficients vs. tip speed ratio of two blades rotors with GBT with a fixed [ARg] (area ratio of inlet and outlet of the GBT) at different width ratios [δ] (ratio between the width of the GBT and the diameter of the rotor) [6]

2.1.9.2. Curtain arrangement

To increase the performance of a Savonius rotor it is important to prevent the negative torque that is formed on the returning blade. According to Altan and Atilgan [21], this is the main purpose of the curtain arrangement, which is a simple wind deflector that increases the performance coefficients and the effects of wind speed without making any modifications in its basic structure.

It is placed in front of the rotor as it can be seen in the Figure 21. In this curtain arrangement the angles *α-β* represents the angles of curtain plates while l_1 and l_2 are the lengths of curtain plates.

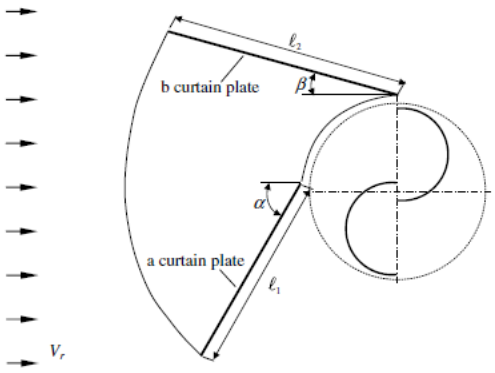

Figure 21 Design of the curtain arrangement placed in front of the Savonius wind rotor [21]

Altan and Atilgan [21] concluded that a rotor with curtain can provide a better performance than a rotor without curtain when the rotor is static at the same angular positions. The results showed that the curtaining with the longest plates is better than the rest and, finally, it was concluded that the optimum angle for the upper plate is 15° on the horizontal axis and 45° for the lower one.

2.1.9.3. *Valve-aided rotor*

In the case of valve-aided rotor, as it is explained by Saha et al. [4], a hole is made on the blade and a rexine cover is pasted on the concave side of the blade so that it can act as a non-return valve. In absence of valves the air strikes on the incoming blade and produces a negative torque against the rotation of the rotor. On the other hand if valves are open, the air passing through it reduces the negative pressure on incoming blade.

A schematic view of a valve-aided blade is shown in the Figure 22.

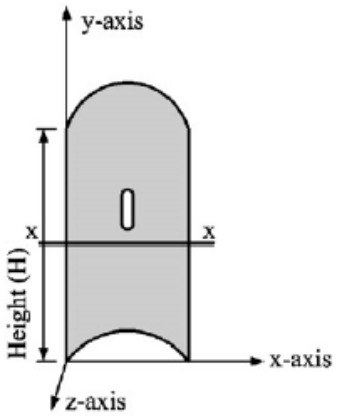

Figure 22 Schematic view of a valve-aided semicircular blade [4]

These additional holes made on blades increases the power coefficients given by the rotor as it can be seen in the Figure 23, where it is noted a comparison between the experimental results obtained with a two-stage three-bladed semicircular rotor and the same rotor with valve-aided blades.

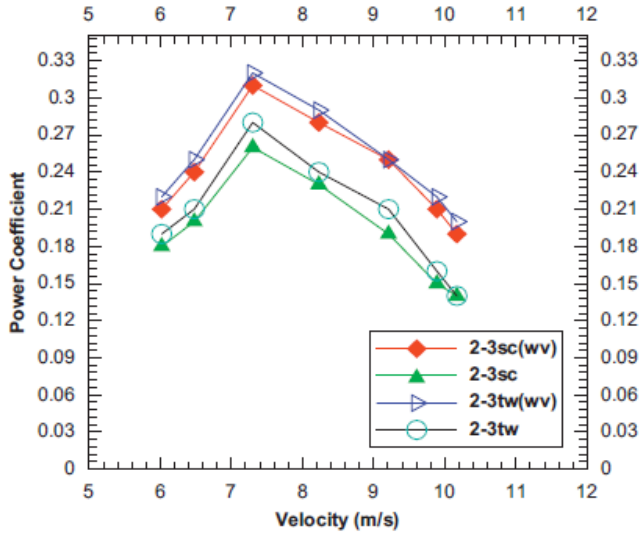

Figure 23 Power coefficient vs. wind velocity for two-stage three-bladed valve-aided Savonius rotor system (sc=semicircular blades, tw=twisted blades, wv=valve-aided) [4]

2.2. Savonius rotor design

2.2.1. Savonius geometry election

After the amount of previous researches analysed and taking into account the space limitations of the wind tunnel that is going to be used in this study, the following rotor configuration is selected (Table 1). It has to be said that the following parameters are preliminary and can be modified later if it is convenient.

Feature	Value	Reason/s according to the bibliography researched
Number of blades	**2**	Gives more efficiency and high power coefficients.
Number of stages	**1**	Does not give the best power coefficients but a single stage rotor is usually smaller and it will fit better in the test bench of the wind tunnel.
Aspect ratio [AR]	**0.77**	Produces high power coefficients.
Overlap ratio [β]	**0.15**	Gives high static torque coefficients and has better aerodynamic performance.
Twist [α]	**12.5°**	Gives high power and torque coefficients, also better performance.
Blade arc angle [ψ]	**124°**	High power coefficients.
Shaft	**Yes**	It Is necessary for holding the rotor with the supports of the test bench.
End plates	**Yes**	Give better aerodynamic performance, high efficiency and they strengthen the structure. Their diameter will be about 10% higher than the rotor diameter [D].
Additional configurations	**No**	There is not enough space in the test bench and they are not included in the main purposes of this experimental study.

Table 1 General features selected for the Savonius wind turbine

2.2.2. Geometry design

Once the most important geometrical properties of the rotor are chosen and justified, a more detailed study of the geometrical features must be done.

First of all, in order to determine the final size and geometry of the Savonius rotor that will be used to carry out the experimental study, the test bench of the wind tunnel located in the Fluid Mechanics Department must be analysed accurately so as to avoid future incompatibilities.

The test bench is defined by three vertical supports placed in a triangular shape as it is shown in the Figure 24.

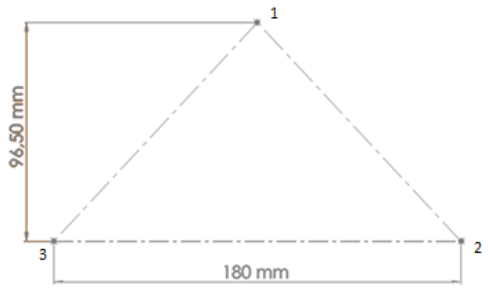

Figure 24 Plan view of the test bench supports position

The supports form a perfect isosceles triangle whose centroid is situated in the middle plane of the wind tunnel outlet. The main idea is to position the rotor horizontally so that its axis is held by the supports 2 and 3, and the purpose of the support 1 will be to fix the rotor in the desired angular position.

Therefore, these three supports establish a rectangular volume where the Savonius rotor has to be placed in. This volume and his measures are represented in the Figure 25.

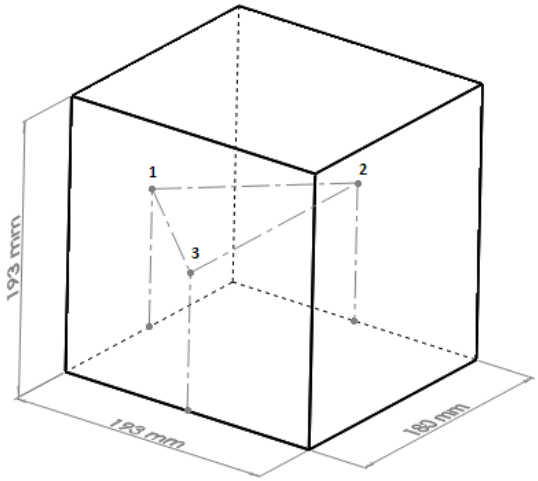

Figure 25 General view of the test bench volume

In the following chapter the supports of the test bench are shown by a 3D representation.

Once the volume that has to contain the rotor is determined, the maximum measures of the Savonius can be defined taking into account the horizontal positioning of the rotor as it has been mentioned before.

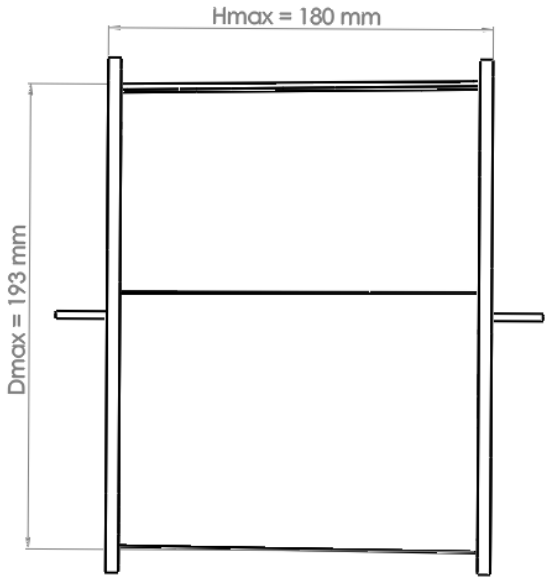

Figure 26 Maximum size of the Savonius rotor

It is necessary to be said that the end plates, as it is shown in the Figure 26, can have a larger diameter than D_{max} because they are located at the extremes of the rotor and they will not hit the support number 1 under any circumstances.

Then these maximum measures, which are defined by the size of the test bench volume described before, are the restrictions for the rotor size. But, logically, the rotor cannot have the same size as the volume because then the blades would rub with the support 1.

Therefore, a little distance has to exist between the three supports and the extremes of the rotor in order to avoid incompatibilities. Hence, a distance was fixed so as to establish a margin of safety between the end plates and the supports 2 and 3 of the test bench.

The value of this margin of safety was chosen to be about 15 mm. Then, to know exactly the needed height of the rotor, the thickness of the end plates has to be defined too and they was agreed to be about 5 mm each.

Therefore, the horizontal size of the Savonius rotor is defined as can be seen in the Figure 27.

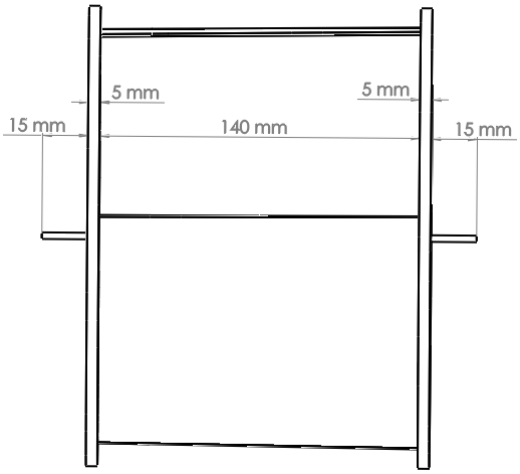

Figure 27 Horizontal size of the Savonius rotor

Thus, the final height of the rotor is:

$$H = 140\ mm$$

Then, to compute the diameter of the rotor [D] with the aspect ratio that has already been chosen:

$$AR = \frac{H}{D} = 0.77 \quad \rightarrow \quad D = \frac{140}{0.77} = 181.82\ mm$$

And finally the diameter of the end plates will be:

$$D_f = 1.1 \cdot D = 200\ mm$$

Now, in order to have the rotor completely defined, the diameter of the blades [d] and the overlap distance [e] have to be calculated. A clear representation of these two parameters is shown in the Figure 28.

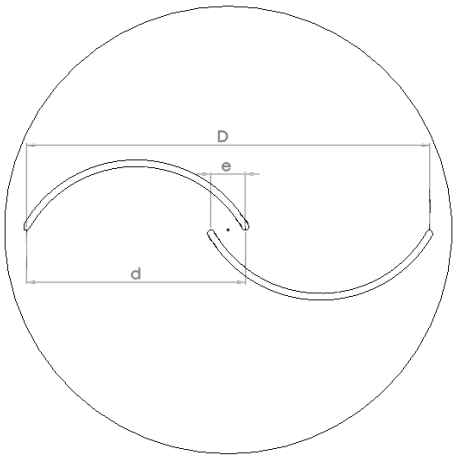

Figure 28 Representation of the overlap distance [e] and the blade diameter [d]. All the measures shown are taken from the middle line of the blade thickness

Firstly, a system of two equations needs to be defined as following:

$$\beta = \frac{e - d_{shaft}}{d} \quad (1)$$

$$D = 2d - e \quad (2)$$

where the overlap ratio [β], which has been defined at the beginning of this chapter, and the diameter of the rotor [D] are known. Hence, the diameter of the shaft must be defined so as to have a system of two equations with two unknowns.

The diameter of the shaft is defined by the metallic pieces situated at the top of supports 2 and 3 of the test bench described before. They establish a shaft diameter of about 2 mm. However, if these pieces are changed later for compatibility reasons between rotor model and test bench, then maybe the shaft diameter needs to be changed too.

Then, if the parameters already known are changed for their respective values, the equations (1) and (2) result as following:

$$0.15 = \frac{e - 2}{d}$$

$$181.82 = 2d - e$$

If the system is solved the results obtained are:

$$d = 99.36\, mm$$

$$e = 16.90\, mm$$

Finally, all parameters needed to determine the rotor geometry are defined. Below it is shown a summary table (Table 2) with all of them:

Feature	Identifier	Value (mm)
Rotor height	*H*	**140.00**
Rotor diameter	*D*	**181.82**
End plates diameter	D_f	**200.00**
Shaft diameter	d_{shaft}	**2.00**
Blades diameter	*d*	**99.36**
Overlap distance	*e*	**16.90**

Table 2 Geometric parameters for the Savonius rotor

2.2.3. Savonius 3D model

Once all the necessary geometrical parameters of the rotor are defined, the next step is to do the 3D model of the rotor in order to make a subsequent 3D printing.

The 3D model has been done by the computer program SolidWorks®, which is a CAD software for mechanical 3D modeling. Also it is important to remark that this software allows us to save the models in STL format, which is essential if a 3D printing is wanted to be done.

It is necessary to say that this 3D model of the Savonius rotor does not include the shaft because a metallic one will be added later for experimental tests.

Then, the final results of the 3D modeling of the Savonius rotor are shown in the Figure 29 and Figure 30.

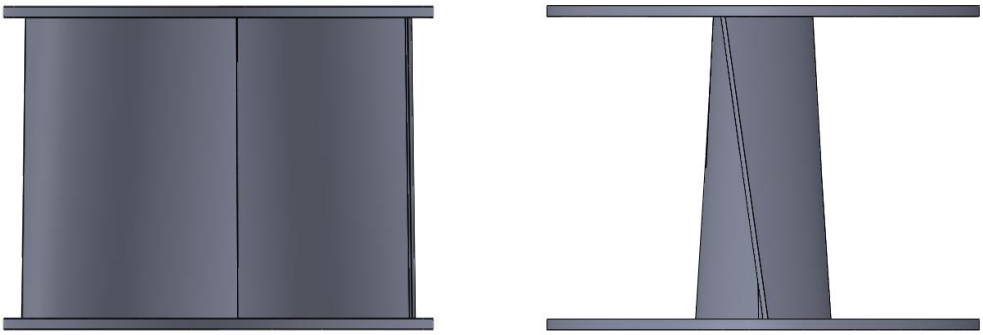

Figure 29 On the left, a frontal view of the 3D model of rotor. On the right, a side view

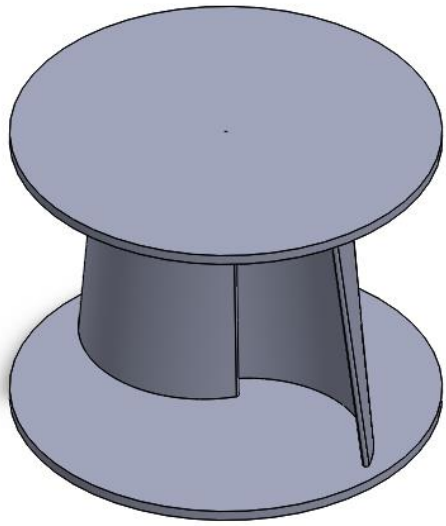

Figure 30 Isometric view of the 3D model of the Savonius rotor

Full measures of the Savonius rotor designed can be found in the Annex I.

It is important to say that the thickness of blades is not the same as the end plates. As mentioned before, the end plates have a thickness of 5 mm whereas the blades have a thickness of 3 mm. This difference exists because of some reasons: firstly it is interesting to have the less weight of the rotor as possible, also because it has to be taken into account the minimum wall thickness that the 3D printer can produce and, finally, because if the thickness was too large then it could affect the geometrical parameters of the rotor.

The 3D model of the test bench was also done using the same CAD software used for the rotor modeling. In the Figure 31 it is shown some views of the final result with the most significant dimensions.

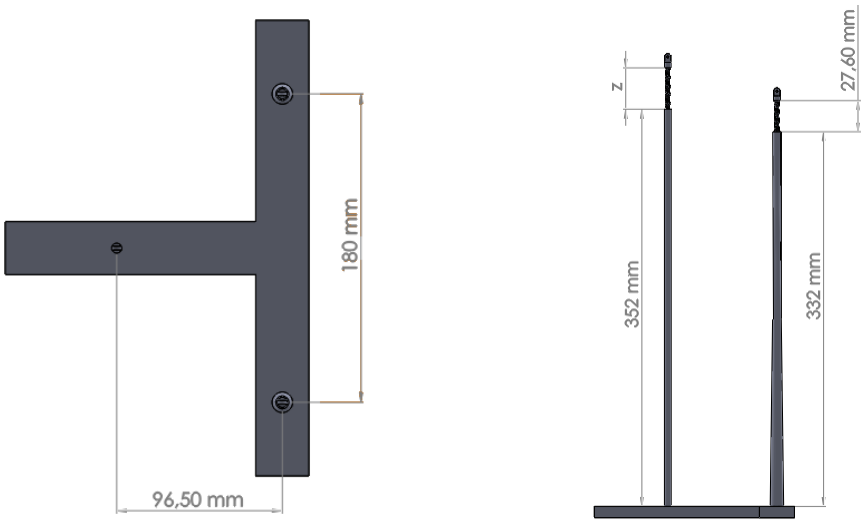

Figure 31 On the left, a top view of the 3D model of the test bench. On the right, a side view

Dimension "Z" in the side view of the test bench shown in Figure 31 above means that this distance is variable and can be modified in order to get the needed length for the rotor fixing system. A global view of the test bench can be seen in the Figure 32.

Figure 32 Isometric view of the 3D model of the test bench

The 3D model of the test bench shown in Figure 31 and Figure 32 has exactly the same dimensions as the real test bench of the wind tunnel of the Fluid Mechanics Department. The main purpose of modeling the test bench is to make sure that the Savonius rotor designed fits on it and, in this way, avoid future incompatibilities.

Finally, the assembly of the 3D model of the rotor and the test bench of the wind tunnel can be noted in the Figure 33.

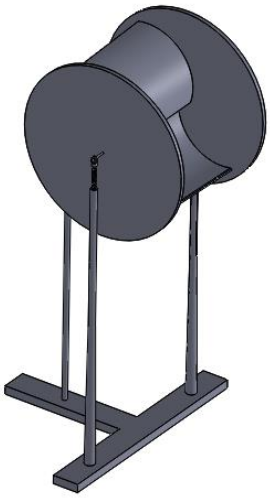

Figure 33 Final assembly of the Savonius rotor and the test bench done with CAD software

2.2.4. Printing process

The 3D printing is composed of two processes, the first one is the generic printing and the following one is the removal process.

The first process is made by a 3D printer situated in the Fluid Mechanics Department. It is a HP Designjet Color 3D Printer (see reference [22]) and builds models from CAD STL files. This printer builds 3D parts by extruding a bead of ABS (Acrylonitrile Butadiene Styrene) material through a computer-controlled extrusion head.

The ABS material is a thermoplastic which is known for its hardness and high impact resistance. It also allows working easily with it.

The 3D printer mentioned builds a maximum part size of 203 x 203 x 152 mm and is able to create a minimum wall thickness of 0.914 mm. Thus, the thickness of the rotor blades and endplates will not be a problem because they are above the minimum thickness specified.

Also, the Savonius rotor, which has a size of 200 x 200 x 150 mm, was printed without troubles. The shaft holes in the endplates were left in order to know their positions in

the future. In addition, the diameter of these holes left were smaller (about 1 mm) than the shaft diameter so as to finish making the holes manually with a drill.

Then, once the 3D printer program has the STL file of the rotor made by CAD software, it makes a preview of the final piece with the support material included as it can be shown in the Figure 34.

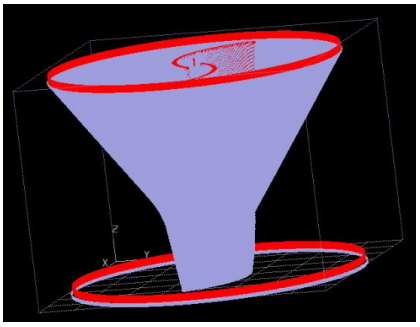

Figure 34 Preview of the final piece made by 3D printer software. Areas in red are ABS material and ones in grey are support material

After the printing time, which was about of 25 hours, the resulting piece was the following (Figure 35).

Figure 35 Final rotor printed with the support material

In Figure 35 the two materials that compose the piece are not clearly distinguished due to their light color.

Hence, in order to remove the support material the next step was the removal process, which was done by HP Designjet 3D Removal System (see reference [23]) situated in the Fluid Mechanics Department. This system removes the support material by immersing the 3D model in a bath of water with a specific amount of cleaning agent bags added previously. The system heats and circulates the solution around the model in the cleaning tank and the solution dissolves the support material without harming the underlying model material. Then, when all the support material is dissolved, the model is ready to be removed, dried and used.

A simplified representation of the main components of the HP Designjet 3D Removal System can be observed in the Figure 36.

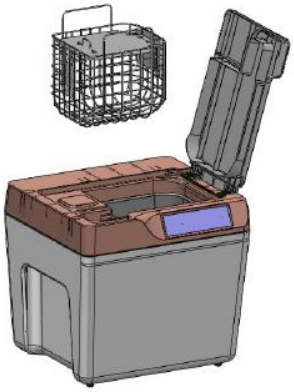

Figure 36 Housing assembly and Dual Level Part Basket of the HP Designjet 3D Removal System [23]

The removal process time was about 12 hours because of the complexity of the model geometry and size. The final result is shown in the Figure 37.

Figure 37 Final rotor printed without the support material

The weight of the Savonius rotor was about 326 grams. It has to be said that the final result was good because of the good quality printing done and the subsequent removal process.

One of the reasons to have a quality printing was to have a high defined STL file. To achieve this it is necessary to create a STL file with a lot of triangles, because as more triangles it has, more accurate the final piece will be.

But on the other hand, it is impossible to obtain a perfect result at the first time, therefore a post treatment of the surface was necessary to be done in order to optimize the finish of the rotor surface.

In addition, some deformations were found in the end plates of the rotor, they were not completely flat but have a small curvature. It was concluded that these deformations were produced due to an inadequate temperature during the 3D printing process, because ABS material needs to be printed in a very specific temperature (between 190 and 200 Celsius degrees according to the reference [24]), and any small change in the temperature can have consequences that can produce deformations in the final piece.

2.2.5. Finishing process

After the printing process and the removal process completed, some small imperfections still remain in the rotor surface. Therefore, as it has been mentioned previously, a post treatment is necessary so as to make the surface smoother and achieve the best surface finish for the aerodynamic study.

These small defects can be small holes, very little lumps or fine scratches. In order to repair and optimize the rotor surface a huge search in the internet was done, but it has to be said that was very difficult to find detailed information about how to treat surfaces of 3D printings due to it is a relatively new topic and there is not specified researches.

Firstly a technique with acetone vapor [25] was found to be the best for ABS pieces and was considered to be carried out, but it was firmly discarded because it produces a loose of definition of details in the surfaces and, in this case, the Savonius rotor printed has to be very accurate. Thus, after talking with some colleagues who have knowledge about the topic, and after searching more information in some forums in the internet, the final process that was decided to be carried out was the following.

The first step was to fill up the surface holes with putty for plastics, but there was the problem that holes were too small and the putty was too dense, for this reason it was very difficult to cover the holes completely. Hence, the putty was not very useful and it was decided to eliminate this step from the finishing process.

Therefore the first step became to sandpaper the rotor surface in order to remove the small defects. It was done with waterproof sandpapers because of the good results they give in ABS pieces. The most imperfections were situated in the blades surface, mainly in the overlap zone where it was very difficult to work in due to the reduced space.

Once all the surface was sandpapered and polished, the next step was to coat the rotor with a fine layer of pure acetone liquid. The acetone is an abrasive liquid that in contact with ABS, it acts melting the most external layer of the surface making it softer and, in this case, making it more suitable for the experimental study. In addition, the acetone acts as a cleaner and as a degreaser of ABS surfaces. The result of the present step is shown in the image (a) of the Figure 38.

The next step was to prepare the rotor for painting. The best way to do so was using a primer for plastics, which is a substance used as a preparatory coat on previously unpainted plastic pieces, especially to prevent the absorption of subsequent layers of paint or the development of rust. In addition, this product firmly recommends the previous usage of acetone in order to prepare adequately the surface. The primer used in this case was white and the result is shown in the image (b) of Figure 38.

a b

Figure 38 View of the Savonius rotor with (a) the acetone applied on its surface and (b) with the plastics primer applied

Finally, the last step was to paint the rotor with an aerosol. The paint color was chosen black because in this way in the case of future visualization studies, the particles held in the air will be seen more clearly if they are on a black background. Hence, the final result after painting the rotor is shown in the Figure 39.

It has to be remarked that the acetone and the primer were applied on the rotor surface with paintbrushes whereas the paint was applied with a spray as it has already been said.

Also it is necessary to note that at the end of the finishing process the weight of the Savonius rotor was about 339 grams, 13 grams more than the rotor freshly printed.

Figure 39 View of the final Savonius rotor after being painted

Now the Savonius rotor is ready for being tested in the experimental tests.

2.3. Experimental study

2.3.1. Introduction

The experimental study consists in two main experiments. Both will be carried out in the Fluid Mechanics Department in wind tunnel facilities.

The first one consists in studying aerodynamic forces (lift and drag) produced by the Savonius rotor for different static angular positions. This experiment will be measured at different wind velocities in order to acquire the necessary data to validate the results obtained. The equipment needed for the present experiment, apart from the wind tunnel as it has been said before, is the wind balance that will allow the measurement of aerodynamic forces over the rotor. In addition, a computer program will be used to prepare adequately the wind balance.

The second experiment consists in the measurement of static torque produced by the Savonius rotor for different angular positions at various wind speeds. This experiment will be carried out in the wind tunnel too, but not with the wind balance because it does not measure the torque correctly. Hence the torque will be acquired with a torque sensor. Moreover, a support structure will be necessary to be designed in order to hold the rotor immersed in air flow because the supports of wind balance do not allow the connection between torque sensor and rotor shaft.

Thus, in order to have more detailed information about the equipment that is going to be used, the most sophisticated devices are described in the following section.

2.3.2. Equipment

Principally the equipment that is going to be used is composed of the wind tunnel and the wind balance both situated in the Fluid Mechanics laboratory. Moreover, another specific device is going to be used in order to carry out the second experiment, the torque sensor, but it will be explained in its corresponding section.

Then the wind tunnel and the wind balance need to be described in detail so as to understand their performance.

2.3.2.1. Wind tunnel

Wind tunnel is a structure which is usually used in the study of aerodynamic effects of airflow around a body. It consists in a tubular infrastructure which contains a fan that produces an airflow that generates aerodynamic forces on the test model situated in the test section as it is described in reference [26].

Exist two types of wind tunnel, there are open-return and closed-return wind tunnels. The first one, which can be named open-circuit too, has an input and an outlet where the circulating air is always different. It is cheaper and also is easier to add products to the air such as flow visualization smoke. However, this model has many disadvantages as the strong effect of environment conditions on the airflow, acoustic pollution due to the fan and the high power consumption. A representation of the main parts of this open type can be seen in the Figure 40.

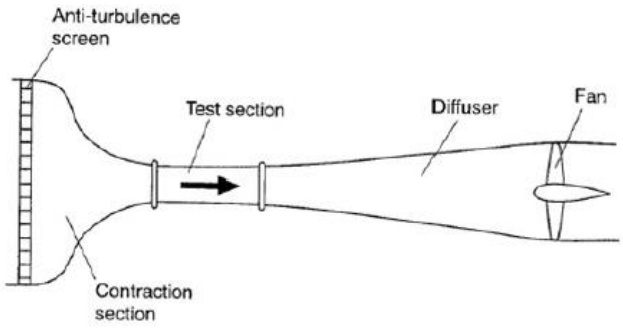

Figure 40 Open-circuit wind tunnel [26]

In the other hand, a closed-return, or close-circuit, wind tunnel is characterized by having the same air flowing through. It requires less energy to be driven in comparison to the open type and it is not sensitive to environment winds. Its main disadvantages are caused by its initial high cost and the increase of temperature because of friction during long turns. It usually has open-jet sections so as to test models and have more accessibility to it.

The wind tunnel placed in the Fluid Mechanics Department is a closed-return type according to reference [26]. It contains an open-test section that allows the placement of the necessary instrumentation such as the balance, the test model, the manometer and the Pitot tube. This test-section is big in order to avoid interferences between airflow and walls, but it has the smallest area so that higher speeds can be reached without increasing the power.

In the Figure 41, image (a) shows a scheme of the main elements that compose the wind tunnel infrastructure. Image (b) shows the real wind tunnel situated in the Fluid Mechanics laboratory.

(a) (b)

Figure 41 (a) Scheme of a close-circuit wind tunnel [26] **and (b) wind tunnel of the Fluid Mechanics Department**

The airflow produced by the wind tunnel can reach speeds up to 60 m/s at full power. In addition, the flow vein wind tunnel has a circular shape of 0.55 m of diameter according to the reference [26]. In this case the maximum speed limitation of 60 m/s is not important because the Savonius rotor will be tested at low wind speeds.

2.3.2.2. Wind balance

In aerodynamic tunnel facilities many applications allow the measurement of aerodynamics forces produced over 3D bodies. Wind balances measure accurately the steady and fluctuating forces that appear on the bodies immersed in a fluid stream. These aerodynamic forces can be calculated with balance geometry and load measurements. When these interacting forces are decoupled, loads over the test model can be represented by six main quantities, three forces and three moments.

According to Raush et al. [27], wind balances can be divided into strain gage, rotary, internal and external. Internal balances, which are usually a stinger, are placed inside the test model attached near its gravity center. They have a low equipment complexity and are able to send the measured data through electrical signals [26]. The model must possess a minimum volume to allow internal balance. Moreover, they are usually used for extremely fast velocities and low drag objects as they only measure the forces acting on the model with a very high degree of accuracy.

In the case of external balances, they are placed out of the air-stream in order to measure the load values applied on the model. Some simulations have demonstrated that this type of balances gives higher accuracy for determining loads than internal ones [26]. However, external balances require a high initial cost due to their equipment complexity. There exist four types that are commonly used. They are classified according to the manner in which the system is assembled: wire, platform, yoke, and pyramidal.

The wind balance of the Fluid Mechanics Department is a 6-component (3 forces and 3 moments) external platform-type balance. It, basically, consists of a T-shape platform resting on six load cells. The balance is installed on the test section of low speed wind

tunnel. As it is described by Raush et al. [27], its working is based on the measurement of six principal forces, three in vertical direction and three in horizontal.

Load cells are used as force-sensing elements based on the strain gage deformation sensors. Force connections between the strain gage cells and the model are achieved using a set of long slender rods (three supports in the present case) fixed to the floating rigid platform. Then a set of specialized flexible elements connects this rigid platform with the load cells.

These elastic elements, which can be elastic hinges, have an important function ensuring the free-floating body condition of the model and its supports and guaranteeing the orthogonality between forces transmitted to the load sensors. A detailed representation of these devices can be seen in the Figure 42.

Figure 42 Detailed view of the elastic rods [27]

The final design of the external wind balance is composed of a central base which is mounted on a circular guide where the load cells are fixed as it is shown in the Figure 43.

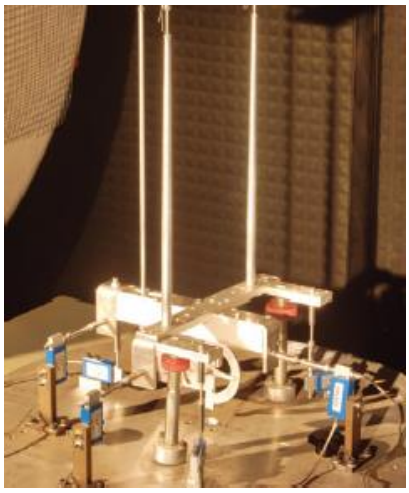

Figure 43 General view of the wind platform balance with all its elements [27]

As it has been mentioned previously, the wind balance contains six load cells that will acquire the data from aerodynamic forces over the model:

- 3 2.5LBF load cells for lift force
- 1 10LBF load cell for drag force
- 2 5LBF load cells for cross-wind (side) force

A clear scheme of the distribution of the six load cells in the wind balance is shown in the Figure 44. Regarding to the moments, pitching moment is the one created by lift and drag force, rolling moment is the moment created by lift and side force, and finally, yawing moment which is the moment created by drag and side force.

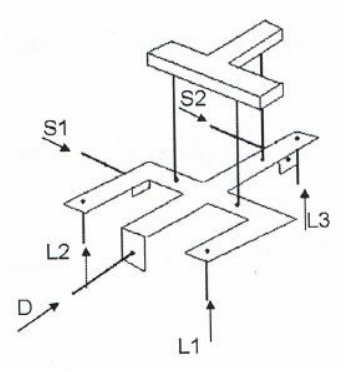

$$Lift: \quad L = L1 + L2 + L3$$

$$Drag: \quad D$$

$$Side\ force: \quad S = S1 + S2$$

Figure 44 Load cells distribution in the wind balance [28]

It is important to remember that force measurements will be valid only if the force orthogonality is conserved. In addition, it has to be said that an accurate calibration process must be done so as to avoid misalignments and moment interactions.

Load cells produce a very small voltage current proportional to load. The sign of the voltage depends on the direction of the load measured. This current has to be amplified and stabilized with a signal conditioner. A SGA model will be used by Interface. The output from this conditioner is a -10V to +10V signal that is read by a data acquisition card in a computer. Specific software gets this data and calculates forces and moments. In addition, it is necessary to say that the dependence between the voltage input and the load measured is linear.

Its load cell sign criteria is the following shown in the Figure 45.

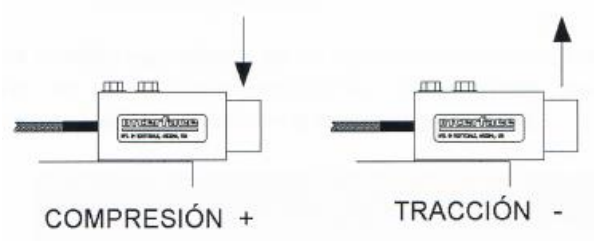

Figure 45 Load cell sign criteria [26]

It is very important not to overload the load cells in order to preserve them, because they require a great investment to be replaced and then a further recalibration of the balance would be required.

But in the present case, the wind balance only can measure the lift force, drag force and pitching moment correctly because some load cells are damaged due to external causes to the present study.

Finally, as it has been mentioned previously, misalignments and deformations in undesired directions could endanger the necessary orthogonality between forces transmitted and loads cells. Hence, the whole structure must allow an axial transmission of aerodynamic forces to the load cells without suffering any kind of beam deflection [26].

2.3.3. Experiment 1: Aerodynamic forces

As it has been explained before, the main purpose of this first experiment is to obtain the aerodynamic forces over the Savonius rotor for different static angular positions at different wind velocities.

The wind speeds which the rotor will be analyzed are 6, 9, 12, 15 and 18 m/s. It can be seen that the velocities are not very high because one of the properties of a Savonius rotor is that it is a low speed wind turbine.

Regarding to the different angular positions, measurements will be carried out every 30 degrees. Moreover, the Savonius rotor will be tested only in the angular positions between 0 and 180 degrees because of the symmetry of the rotor. This means that the angular positions at which the Savonius will be studied are 0, 30, 60, 90, 120 and 150 degrees. The angular position of 180 degrees will not be tested because, theoretically, it will provide the same results as the position 0 due to the rotor symmetry.

The angular position will be defined from the central section of the blades (middle point of the blades height) because of rotor twist.

The reference angular position is 0 degrees, which is when the line drawn by the central section of blades is parallel to the input air stream. In the Figure 46 it is shown a clear representation of the angular position [θ], its defining geometric lines and its direction of rotation.

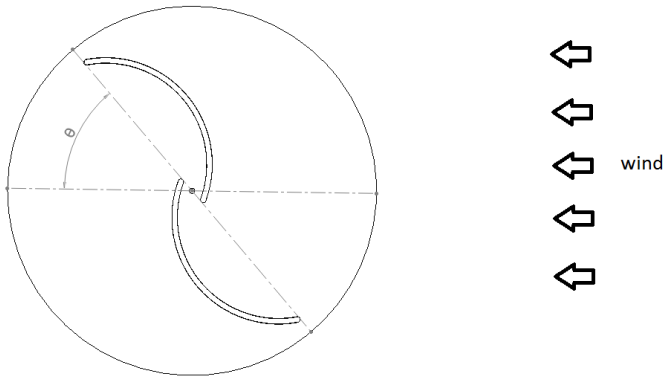

Figure 46 Scheme of the angular position [θ] defined by the Savonius rotor

In the following section, the fixing system of the rotor on the wind balance and the angular positioning system are described.

2.3.3.1. Rotor fixing system

In order to fix the Savonius rotor in the wind balance of wind tunnel, it is necessary to find the optimum fixing system that gives the best performance needed for the experimental study.

First of all, it was found that a shaft of 2 mm of diameter was too small and also it was very difficult to find a metallic shaft of these characteristics in the market. Hence, a threaded shaft of 3 mm of diameter was decided to be used, because it is more used commercially and it is more resistant. In addition, a threaded shaft, instead of a non-threaded one, will facilitate screwing the rotor in the wind balance supports.

Therefore, if the shaft diameter changes, the Overlap ratio [β] changes too because it is a geometric parameter that takes into account the diameter of the shaft used in the Savonius rotor.

Previously, the value of the Overlap ratio was defined as 0.15 because of the bibliography researched. However, it is necessary to remember that in the geometrical study done there was a big disagreement between researchers in which was the optimum value for this parameter. Some of them said that the best one was 0.15, others between 0.2 and 0.3, and others that the Overlap ratio is not necessary. But finally the value of 0.15 was chosen for the present experiment.

Now with a new shaft diameter of 3 mm, a new value of Overlap ratio will be obtained according to the equation (1). Values of *e* and *d* are already defined because the Savonius rotor is already printed and his geometry cannot be modified. The values of these parameters are summarized in the Table 3.

Feature	Identifier	Value (mm)
Shaft diameter	d_{shaft}	**3.00**
Blades diameter	*d*	**99.36**
Overlap distance	*e*	**16.90**

Table 3 Predefined geometric features and the new value of shaft diameter

Hence the value of the final Overlap ratio according to (1) is the following:

$$\boldsymbol{\beta} = \frac{16.90 - 3.00}{99.36} = \mathbf{0.14}$$

It can be seen that the new number obtained is not so much different of the previous. This can be interpreted in the way that the shaft diameter change should not have a great effect in the Savonius rotor performance. Moreover, Ohara et al. [29] showed that the most efficient configuration was found when the overlap ratio of rotor in operation took a value of 0.14.

Now that all geometrical parameters are definitely fixed, it is necessary to define the fixing system which will be used in order to carry out the experimental study.

As it has been said previously, two holes of 1 mm of diameter were left in the end plates during the printing process so as to mark the future pass of a metallic shaft. Therefore, the first step is to make the appropriate holes in the end plates. Both holes were made with a vertical drill in the Fluid Mechanics Department with the corresponding safety conditions. A bit of 3 mm of diameter was used.

Then, after checking that the threaded shaft crossed the rotor holes correctly, the next step is to tighten it to the rotor with adequate nuts and packing rings both of 3 mm of diameter according to the shaft size. It has to be said that the shaft was only screwed to the rotor on the outside of the end plates, because inside there was not enough space to place a nut or a packing ring due to the small overlap distance between blades.

Once the shaft rotor assembly is fixed, it is needed to define the fixing system between the shaft and the two symmetric supports of the wind balance. This system was done with a metallic piece which allowed a perfect attachment between elements mentioned. The metallic piece used is shown in the Figure 47.

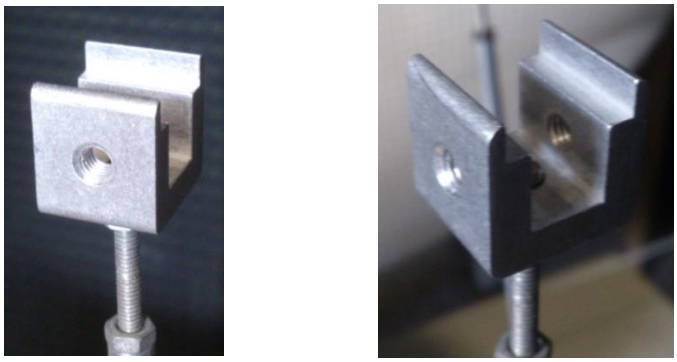

Figure 47 Metallic piece used to fix the threaded shaft in the wind balance supports

It can be seen in Figure 47 that the metallic piece has a quite complex geometry, because it has two threaded holes in its vertical plane and another in its horizontal plane. It also has to be said that, luckily, there were enough of these pieces in the Fluid Mechanics Department and it was not necessary to request more.

Then, with one of these pieces properly screwed on each support of the wind balance, the result was the following shown in the Figure 48.

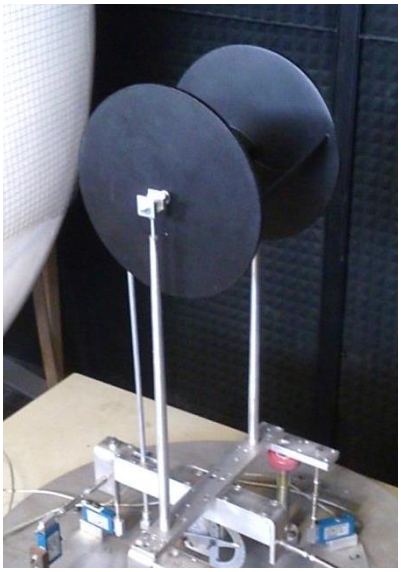

Figure 48 Savonius rotor fixed on the wind balance supports

The junction between shaft and the metallic pieces was made by nuts and packing rings both with the suitable size according to the shaft diameter of 3 mm. It is necessary to add that a double nut was placed on the shaft ends in order to make the assembly more resistant. Moreover, empty spaces left in the shaft between metallic pieces and rotor end plates were filled with nuts so as to strengthen the structure and make it more compact.

The final length of the metallic shaft used was about 218 mm.

Although all the nuts and packing rings used to fix the Savonius rotor to the wind balance supports, the rotor still rotated when an air stream passed through its blades. Hence, another fixing system had to be defined in order to remove the rotor rotation and allow testing the Savonius rotor at different static angular positions.

2.3.3.2. Angular positioning system

The third support of the wind balance was used to design the angular positioning system (APS), which has to allow studying the Savonius rotor in different static angular positions (every 30 degrees, from 0 to 150) as it has been explained before.

A 3D representation of the system designed made by CAD software is shown in the Figure 49.

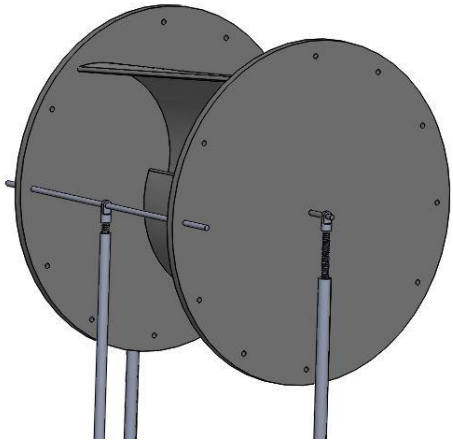

Figure 49 3D model of the angular positioning system designed for experiment 1

The system is based in a threaded metallic rod (like the rod used as rotor shaft) which attaches the third balance support with the end plates of the rotor through some holes made in it.

Regarding to the figure above, the pieces shown that attaches the supports with the two threaded metallic rods are not the ones used for the present experiment, the real pieces used (even by the third support) are the metallic pieces shown in Figure 47.

Then, in order to make the corresponding holes in the end plates of the rotor, a real measure template was made. That template had the same size as the end plate diameter and, obviously, had a radial line every 30 degrees so as to define correctly the holes position. These positions formed a circumference whose diameter was equal to the diameter of the rotor [D] which was already defined.

If a look is taken in the figure above, it can be seen that in the angular positions of 0 degrees there is no hole, this is because it would coincide with blades position and therefore it would damage the structure and geometry of blades. Hence, another system was necessary to be designed in order to study the aerodynamic forces of the Savonius rotor in this angular position. This system will be described below.

The next step was to mark the holes positions on the surface of both end plates with the help of the template described above. Then the corresponding holes were made with the same vertical drill and the same bit used for the shaft holes, as the threaded metallic rod used for this system had the same diameter as the rotor shaft, equal to 3 mm.

It is important to highlight that only the holes corresponding to the angular positions 30, 60, 90, 120 and 150 degrees were made because of the symmetry of the experiment as it has been mentioned previously. Then, the final result of the Savonius rotor assembled to the wind balance with the APS attached is shown in the Figure 50.

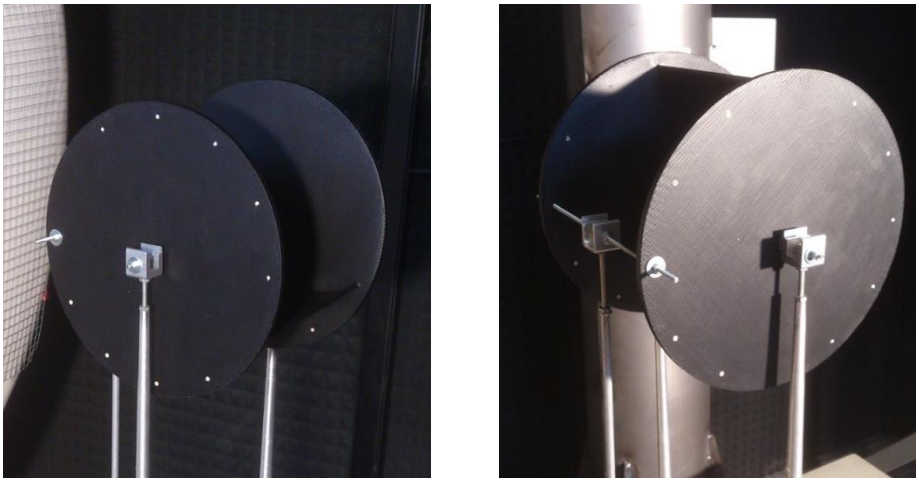

Figure 50 Final assembly of the Savonius rotor to the wind balance

It can be seen in Figure 50 that the three supports are at the same height, this is because the angular positions will be measured regarding to the horizontal plane, which is how the system had been thought initially and, in this way, it will be easier to know at what angular position the rotor is being tested in each moment.

Therefore, looking at Figure 50 it is possible to know exactly at what angular position the rotor is fixed counting white holes and taking into account the direction of rotation, which is already established. In the picture on the left the Savonius rotor is fixed in the position of 30 degrees because the APS is attached in the first hole. In the other hand the picture on the right shows that the rotor is fixed in the position of 90 degrees because the APS is attached in the third hole.

As it can be seen in the Figure 51, the APS also includes some nuts and packing rings which make the system more compact and avoid possible vibrations between the rotor and the third support of the wind balance.

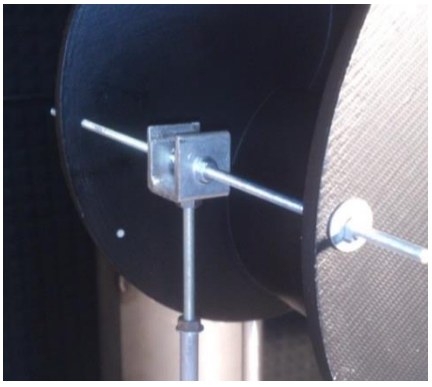

Figure 51 Detailed view of the angular positioning system (APS)

In order to fix the rotor in the angular position of 0 degrees, a very simple system was used. Because in this case which the Savonius is positioned totally horizontal, the holes of 90 degrees are situated in front of the two symmetric balance supports. Therefore a

metallic wire was used to join both elements and, in this way, fix the Savonius rotor at this angular position. It has to be said that however the simplicity of the system, the metallic wire was resistant enough to maintain the angular position during the tests.

Once the Savonius wind turbine is completely fixed to the wind balance with both systems described above, the next step is to explain the procedure that has been followed to carry out the experiment.

2.3.3.3. Interfaces

It is very important to keep the wind balance and the wind tunnel operative. The wind tunnel is controlled by a control device which is directly connected with it. This device, as it is shown in the Figure 52, has a button (in green) to turn on the wind tunnel motor, another one (in red) to turn off it, and finally a power regulator that allows to control the power of wind tunnel engine.

Figure 52 Controller of the wind tunnel

In the other hand, the control of the wind balance is a bit more complex because it needs software in order to acquire the necessary data. In the Fluid Mechanics Department the software used is LabVIEW (Laboratory Virtual Instrument Engineering Workbench) which implements platforms such as signal processing, data acquisition or instrument control according to [26]. As it has been explained before, the load cells transform the loads they receive in electric signals (from -10V to +10V), and then these signals are received by the data acquisition card of the LabVIEW software which analyzes them and gives a final result through the computer screen.

In this case, the LabVIEW software is implemented in a computer situated next to the wind tunnel. It has the necessary connections to the load cells of the wind balance so as to acquire their data.

The LabVIEW program used for the present experiment is one called "*practice_balance*" which was already done and is still in use to make laboratory practices related to aerodynamic forces produced by an airfoil in the wind tunnel. Hence, this program that is going to be used is already prepared to calculate aerodynamic forces over a 3D body. This means that it will not be necessary to modify the program code to carry out the present study.

First of all, it has to make sure that the wind balance is connected to electric system and also wait a few minutes after starting tests so as to let the balance get ready. Then when the program "*practice_balance*" mentioned above is shown operative in the computer screen, the first step is to tare the load cells in order to avoid the measurement of balance weight, the weight of the 3D body, and other components like, in this case, rods and fixing elements. The tare interface, called "*Tarado*", of the LabVIEW program is shown in the Figure 53.

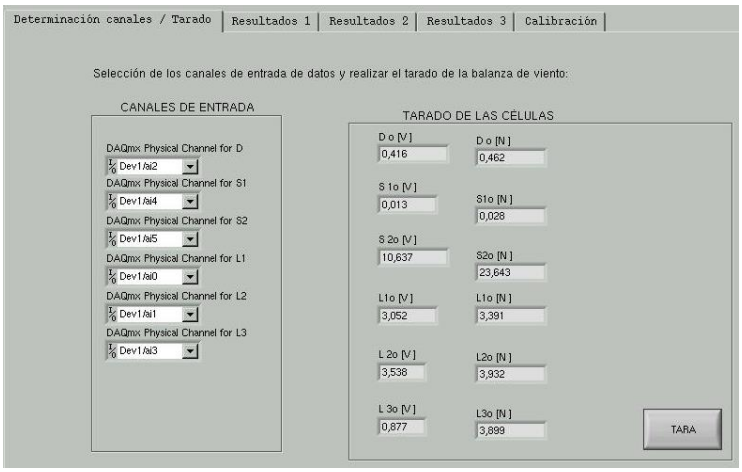

Figure 53 Tare interface in LabVIEW

It is necessary to remember that any modification in the 3D body or any additional element in the wind balance will require a new tare before any measurement.

Then wind tunnel can be turned on, a wind velocity also must be defined rotating the power regulator and, finally, acquire the data measured by load cells of the balance. In order to achieve the data acquisition, the interface needed is "*Resultados 1*" which is shown in the Figure 54.

Figure 54 Data acquisition interface in LabVIEW

In Figure 54 it can be seen two main tables which show data about values of voltage and forces given by load cells. But the important element of this interface is the button on

the top with the word "*Valores*", which allows the data acquisition of load cells clicking on it a few times, three or four are enough. This is done to iterate the load cells measurements taking into account their wear and, in this way, obtain more realistic values.

Then, once "*Valores*" button has been pressed several times, next step is move to the interface called "*Calibración*" which shows the final iterated results of the forces measured by load cells. This interface is shown in the Figure 55.

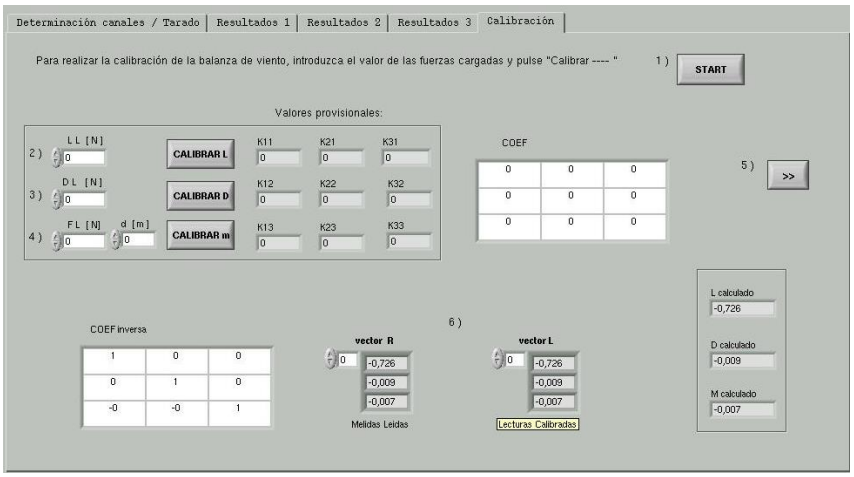

Figure 55 Results interface in LabVIEW

Finally, in order to see the final measured values it is necessary to click on the button on the right with number 5. Then final results will be shown in the table on the bottom right corner, which gives the aerodynamic forces (lift and drag) in (N). This table also shows the momentum calculated but it cannot be considered for the study because the value given is wrong due to internal errors of the program code.

Fortunately, the values of lift and drag, which are the necessary results for the present experiment, are given correctly. A sample of the results table with random values is shown in the Figure 56.

Figure 56 Results table in LabVIEW

In Figure 56 it is also possible to see that the values are given with their respective signs, therefore it is important to define the sign criteria of aerodynamic loads according to

wind balance. The sign criteria used is the same as most of aerodynamic studies, lift is positive when its direction is upward and, in the case of drag, when its direction is backward as it is shown in the Figure 57.

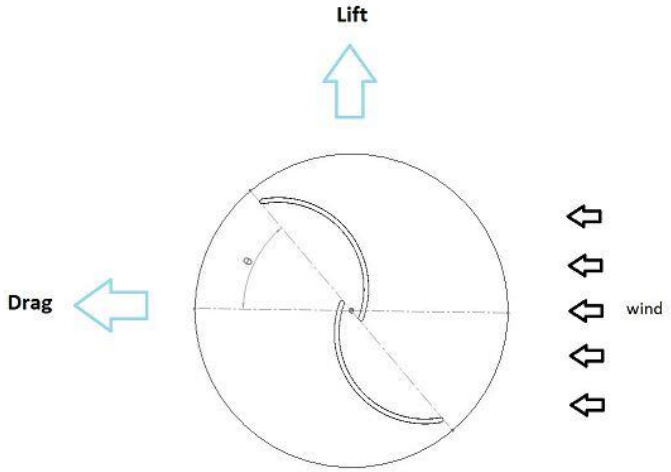

Figure 57 Sign criteria of aerodynamic forces over the Savonius rotor

In any experimental study the values measured will have an error because of experimental inaccuracies. This error must be taken into account in order to achieve an acceptable approximation of the real value. In the present case, main errors can come from possible vibrations during the tests, misalignments in wind balance, and undesirable deformations in load cells. Therefore, experimental errors are implicit in the measurements and they cannot be omitted.

The error considered for this experiment will be explained in the following section.

2.3.3.4. Experimental process

After all the facilities, fixing systems and interfaces defined, it is time to explain the process followed in the laboratory to carry out the experimental tests.

As it has been said in the beginning of this experiment, wind velocities which are going to be tested in the wind tunnel are 6, 9, 12, 15 and 18 m/s. These velocities must be defined with the power regulator of the control device of wind tunnel. But it is impossible to establish a precise wind speed only using that regulator because it has a numbered scale (Figure 58) which defines the power given by the wind tunnel engine.

Figure 58 Numbered scale of the power regulator of the wind tunnel

Hence, it is necessary an additional device to know exactly at what speed the wind tunnel is testing. This additional velocity measurement device is a Prandtl tube [30], or a Pitot static probe, which measures the difference between the total pressure in the point, p_0, and the static pressure, p, as it can be seen in the Figure 59.

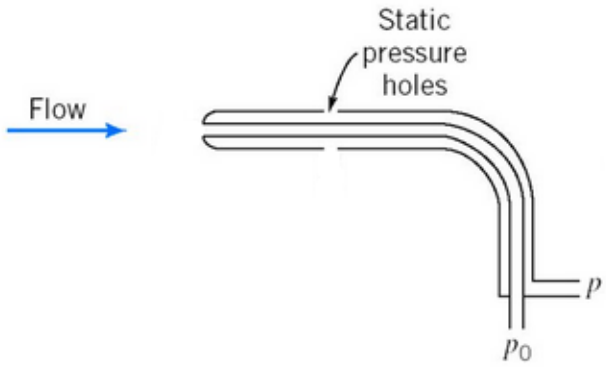

Figure 59 Scheme of a Pitot static probe [31]

Then the air velocity can be calculated with,

$$V = \sqrt{\frac{2(p_0 - p)}{\rho}} \tag{3}$$

where ρ is the air density. The relative total pressure $\Delta p = (p_0 - p)$ is measured with an inclined alcohol manometer. Considering that the inclination angle of the manometer is γ, and ρ_{man} is the density of the alcohol. Thus, the relative total pressure is calculated as:

$$\Delta p = (p_0 - p) = \rho_{man}\, g\, \Delta l\, sin\gamma \tag{4}$$

where $\Delta l = (l - l_0)$ is the length of the manometric fluid column, related to the initial length l_0, which is the position of the column when there is no flow and, finally, g which is the gravity. The values of all parameters needed to determine the air speed are summarized in the Table 4.

Feature	Identifier	Value
Laboratory temperature (ºC)	*Temp*	**20**
Air density (kg/m^3)	*ρ*	**1.225**
Alcohol density (kg/m^3)	*ρ_{man}*	**784**
Inclination angle (°)	*γ*	**30**
Initial length (mm)	*l_0*	**0**
Gravity (m/s^2)	*g*	**9.81**

Table 4 Summary of all fixed parameters during the laboratory tests

It is necessary to remark that the adjustment of the probe angle has not been applied in wind speed measurements.

Now, with all these parameters fixed and the equations shown above, it is possible to relate the velocities which have been defined previously with the necessary length of alcohol column in the manometer. The alcohol column length corresponding to each air speed is shown in the Table 5.

V (m/s)	V (km/h)	l (mm)
6	*21.6*	**5.7**
9	*32.4*	**12.9**
12	*43.2*	**22.9**
15	*54*	**35.8**
18	*64.8*	**51.6**

Table 5 Relation between test speeds and its corresponding length of alcohol column

Then, it only will be required to rotate the power regulator until the alcohol column achieves the calculated length for each air speed. It is necessary to say that abrupt rotations in the power regulator must not be done because they could damage the performance of wind tunnel or control device, hence the power regulator must be rotated smoothly.

Once the wind speed is defined according to the alcohol manometer, the Savonius rotor is correctly fixed in the wind balance, the angular positioning system is fixed in the desired angular position, the wind balance and the wind tunnel are connected to the electric system and LabVIEW is operative in the computer screen, the results acquisition can start.

This process must be repeated until the Savonius rotor has been tested for all angular positions and all wind velocities.

During the experiment, the wind balance was tared after each angular position change so as to avoid possible errors. During these changes, it was completely important not to produce additional loads to the wind balance due to the high sensitivity of load cells.

Now that all the components used in this experiment have been explained in detail, a schematic diagram of the experiment setup and some interesting measurements (in mm) can be seen in the Figure 60.

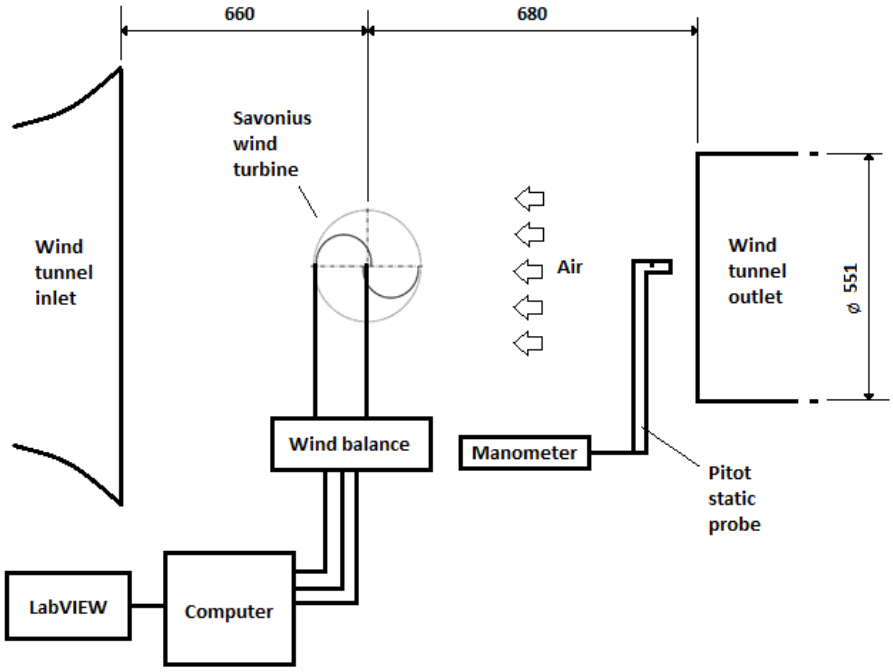

Figure 60 Schematic diagram of experiment setup with some measurements in mm

All angular positions tested are shown in the Figure 61.

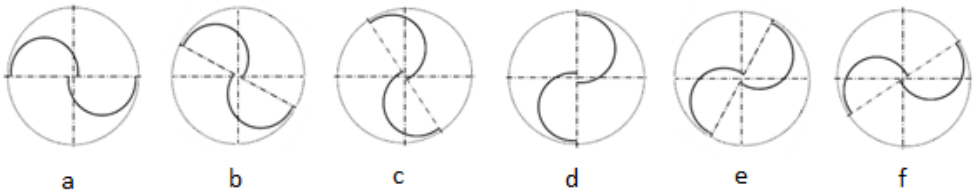

Figure 61 Rotor positions (a) 0/180°, (b) 30°, (c) 60°, (d) 90°, (e) 120° and (f) 150°

Before seeing all the results, it is necessary to remember some important issues.

The results obtained by LabVIEW are given in (N) because they are aerodynamic forces, hence in order to make the post processing more accurately it is necessary to study the results with dimensionless coefficients.

In the present experiment, lift and drag coefficients are going to be used and each one is defined as following.

Lift coefficient is calculated from:

$$C_L = \frac{L}{\frac{1}{2}\rho V^2 A_s} \tag{5}$$

where L is the lift force given by the wind balance in (N), ρ is the air density in (kg/m^3), V is the air speed in (m/s) and A_s the swept area of the rotor in (m^2) which is calculated as:

$$A_s = H \cdot D \tag{6}$$

Drag coefficient has the same formula but replacing the lift force by the drag force in (N) too.

$$C_D = \frac{D}{\frac{1}{2}\rho V^2 A_s} \tag{7}$$

Also, another interesting dimensionless coefficient is the Reynolds number [Re], which is used to plot some graphics in the following section. Therefore it is necessary to introduce how this parameter is defined:

$$Re = \frac{VD}{\nu} \tag{8}$$

where V is the air speed in (m/s), D is the diameter of the rotor in (m) and ν is the kinematic viscosity of the air in (m^2/s) equal to 1.5e-5. Reynolds numbers corresponding to wind velocities that have been tested in this study are shown in the Table 6.

V (m/s)	Re
6	*72728*
9	*109092*
12	*145456*
15	*181820*
18	*218184*

Table 6 Reynolds numbers tested

2.3.3.5. Results

First of all, it has to be said that all the results obtained from experiment 1 can be fully found in the Annex II.

It is important to remember that it must be considered an error about 6-7% in the wind balance measurements due to possible misalignments between the balance structure and the six load cells and also due to possible vibrations during the data acquisition.

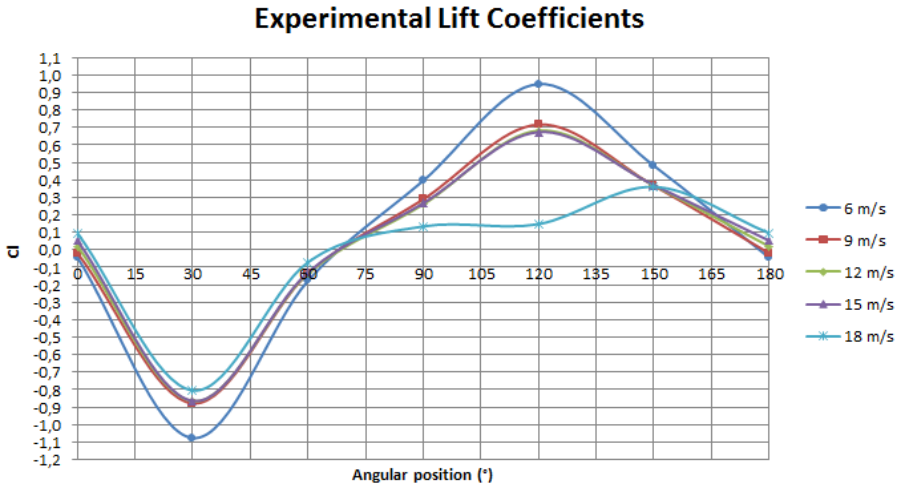

Figure 62 Experimental lift coefficients versus phase angle

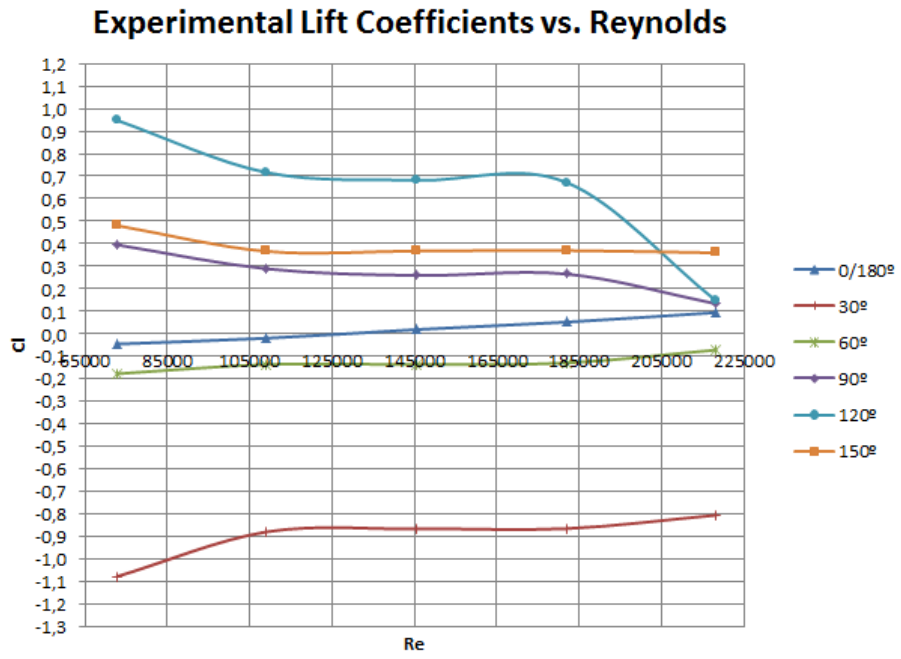

Figure 63 Experimental lift coefficients versus Reynolds number

In the Figure 62, it is observed that, independently from air velocity, all the curves have almost the same values except in the case of the biggest speed, 18 m/s, which in angle range from 90 to 150 degrees it has lower lift coefficients than the other velocities.

This fact is also observed in Figure 63, where it is noted that all lift coefficients remain quite constant with the increment of Reynolds number, except in the case of the biggest Reynolds in the curve of 120°, which has a lower value. In addition, it can be seen that at the lowest Reynolds, almost all lift coefficients diverge a little from the straight line followed by the other values of each curve. Theoretically, all the results should be constant along Reynolds number range.

But in general, there is no significant effect of Reynolds number on the results of lift coefficients obtained.

Regarding to Figure 62, the minimum of all curves is produced in the phase angle of 30 degrees whereas the maximum is produced in the phase angle of 120. The pattern followed by almost all curves can be described in a first decline to negative values in the angle range between 0 and 30, then an approximately linear increase changing from negative to positive C_L values in the range between 30 and 120 degrees, and a final decline in the angle range included between 120 and 180 degrees.

It is noted that the minimum value of lift coefficient is about -1.1 produced in the case of 6 m/s, the lower velocity tested. The other minimums of the rest of air speeds tested have values between -0.9 and -0.8.

The maximum value of all the curves is the one produced in the case of 6 m/s and is about 0.95. Another time the rest of maximum coefficients of the other wind velocities have lower values included from 0.67 to 0.72. In exception of the biggest air velocity, 18 m/s, which in the phase angle where the other velocities have their maximum, the phase angle of 120° has a much lower value.

This exception at the velocity of 18 m/s (Re=218184) is observed in both figures above. It could be produced by a misreading of lift force acquired by load cells due to small vibrations in the wind balance, because it is necessary to say that during the test at the air speed of 18 m/s some vertical vibrations were observed in the wind balance structure at the phase angles of 90 and 120°.

Drag coefficients, C_D, obtained are the following.

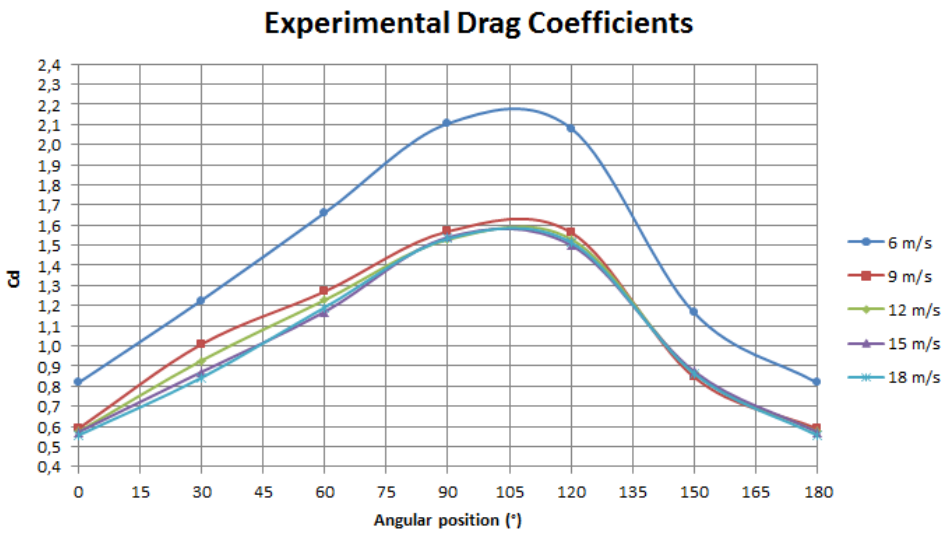

Figure 64 Experimental drag coefficients versus phase angle

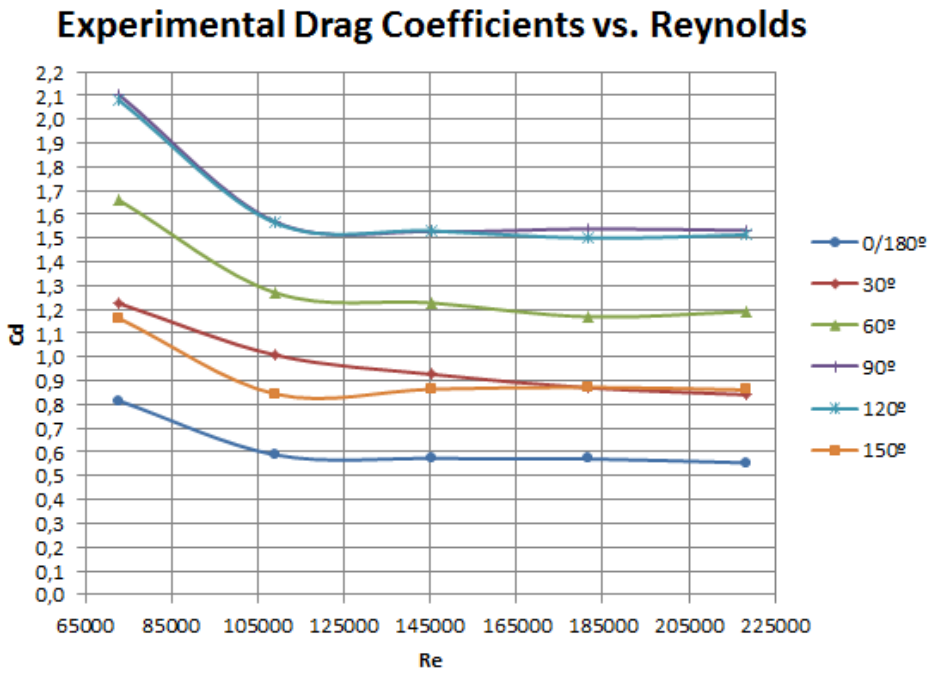

Figure 65 Drag coefficient versus Reynolds number

In the Figure 64 it is noted that, as C_L results, drag coefficients are independently from the wind speed because almost all the curves have the same values. This is very clear in the Figure 65 where all the results remain constant in all the Reynolds number range except in the case of 6 m/s which has higher values than the rest. Theoretically, all the results should be constant without exception as it has been said before.

Regarding to Figure 64, it can be observed that the minimum drag coefficients of all curves are produced in the phase angle of 0/180 degrees whereas the maximum is produced in the phase angle of about 110°. It is also remarkable that all the values are positive at any phase angle.

The pattern followed by exactly all the curves is described as a first gradual increase in the angle range between 0 and 90, then the maximum which is produced in the range between 90 and 120 degrees, and a final steep curved decline in the angle range included between 120 and 180 degrees.

This pattern described has aerodynamic sense because as the Savonius rotor rotates increasing its angular position, from 0 to 90° approximately, the convex and concave surfaces of each blade are being positioned perpendicular to the air flow increasing the swept surface and, therefore, the drag force. Then after the phase angle of 120°, the swept surface decreases until the initial angular position of 0/180°.

The minimum value of drag coefficient is about 0.6 produced in all cases except at the velocity of 6 m/s, which has a minimum of about 0.8.

Then, the maximum value of all curves is the same for all velocities and is about 1.6 except in the case of 6 m/s, which has a maximum drag coefficient near 2.2. It is remarkable to see that in both coefficients graphics, C_L and C_D, the results obtained at 6 m/s are higher than the ones obtained by the rest of wind velocities.

In difference with C_L results, drag coefficients obtained at 18 m/s follow the same pattern as the rest. This is because the small vibrations observed in the tests at 18 m/s appeared only in the vertical direction and, in this way, they did not affect the measurement of the drag force.

2.3.3.6. Experimental results comparison

The experimental results obtained by the aerodynamic tests carried out in the Fluid Mechanics Department are going to be compared in three different ways:

- Experimental study of aerodynamic forces over a Savonius wind turbine carried out by Irabu and Roy [32].
- Numerical study with CFD of aerodynamic forces over a Savonius wind turbine carried out by Martorell [33].
- Theoretical study of aerodynamic forces over a Savonius wind turbine.

The first experimental study mentioned has been carried out with a Savonius rotor which has similar geometrical features with the one designed in the present study. The geometrical parameters of that Savonius rotor are summarized in the Table 7.

Feature	Value
Number of blades	**2**
Number of stages	**1**
Aspect ratio [AR]*	**1.91**
Overlap ratio [β]*	**0.14**
Twist [α]*	**0°**
Blade arc angle [ψ]*	**180°**
Shaft	**Yes**
End plates	**Yes**

Feature	Identifier	Value (mm)
Rotor height	*H**	**220.00**
Rotor diameter	*D**	**115.20**
End plates diameter	D_f*	**170.00**
Shaft diameter	d_{shaft}*	**4.00**
Blades diameter	*d**	**64.00**
Overlap distance	*e**	**12.8**

Table 7 Geometrical parameters of the Savonius rotor used in [32]

It is also necessary to say that in the experiment carried out by Irabu and Roy the Savonius wind turbine was tested horizontally, in other words, with the rotation axis positioned parallel to the horizontal plane, like the tests carried out in this study.

In the case of the study carried out by Martorell, the Savonius rotor used is exactly the same as the present study. Hence, there will not be problems to compare the results obtained by each work. In addition, these results provided by Martorell will be very important in order to validate the results obtained experimentally.

In the theoretical study the Savonius rotor of this project is going to be analyzed so as to compute aerodynamic forces theoretically.

2.3.3.6.1. Experimental study comparison

In this section the results obtained in the present experiment, C_L and C_D, are going to be analyzed in comparison with the results obtained by Irabu and Roy [32].

The C_L and C_D results extracted from [32] are defined with the same equations as the ones used in the present study, with the same swept area definition. Both results are presented in the Figure 66.

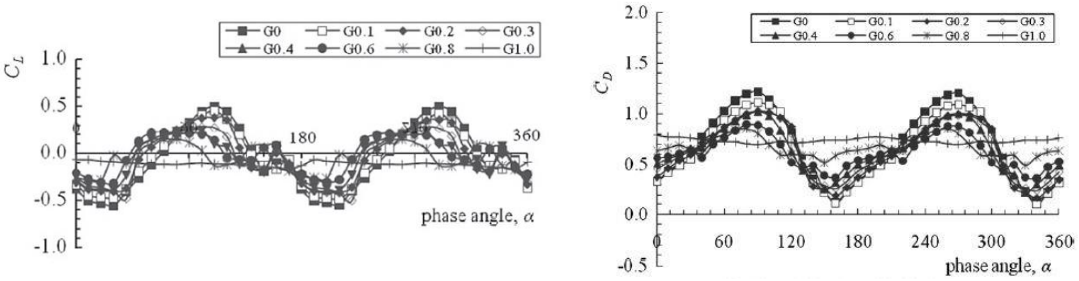

Figure 66 Lift and drag coefficients versus phase angle [32]

It is important to say that the results shown in Figure 66 were tested at an air velocity of about 6 m/s. Their legends describe different overlap ratios (*G* in the plots above) used for testing the Savonius rotor.

The interesting curves are the ones named "G0.2" from the legend, which means that the overlap ratio has a value equal to 0.2. But this value is defined according to the definition of overlap ratio made in [32], which is different from the definition made in the present study. If this overlap ratio is calculated like the way used in this study with the equation (1), then it results:

$$\beta^* = \frac{e^* - d^*_{shaft}}{d^*} = \frac{12.8 - 4}{64} \approx \mathbf{0.14}$$

as the overlap ratio defined in Table 7 above.

Then, in order to compare the results in a more appropriate way, the *x* axis of both coefficients shown in Figure 66 are going to be reduced to the range from 0° to 180° because of the symmetry between the two periods of 180° observed in the whole cycle.

Firstly, the comparison of lift coefficients can be seen in the Figure 67.

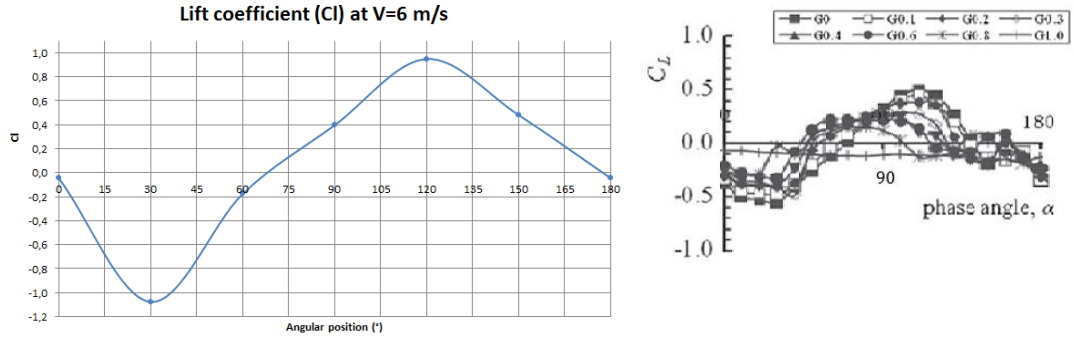

(a) (b)

Figure 67 Comparison between lift coefficients obtained in (a) this experiment and (b) Irabu and Roy [32]

In Figure 67 it is noted that the pattern followed by both curves are quite similar. Results obtained in (b) show a curve with not as much smooth slopes as (a), but this is because in (b) the values have been measured at every 10° of the phase angle of blade and, hence, the curve has many more points and can be defined with more accuracy.

The first difference that can be seen between both graphics is that in (b) the phase angle of 0° gives a negative value of lift coefficient of about -0.3 approximately, whereas the results in (a) gives a value near to 0.

The minimum and maximum values are also very different. Plot (b) shows a minimum value near -0.5 at the phase angle of 35° approximately, a value which is far from the minimum lift coefficient of -1.1 obtained at 30° in (a). Maximum in (b) is about 0.4 at the phase angle near 120° whereas the maximum in (a) is about 0.95 at the same angular position. But these maximum and minimum aspects are not very significant because of the high values obtained at 6 m/s in Figure 62 in comparison with the rest of wind speeds.

In conclusion, it is clear that differences between results mentioned above are mainly due to the different geometrical features between both Savonius rotors, such as the aspect ratio and the blade arc angle, because both studies have been carried out with very similar test conditions, such as the air velocity of 6 m/s and the rotor position regarding to the air flow.

Then the following step is to compare drag coefficient.

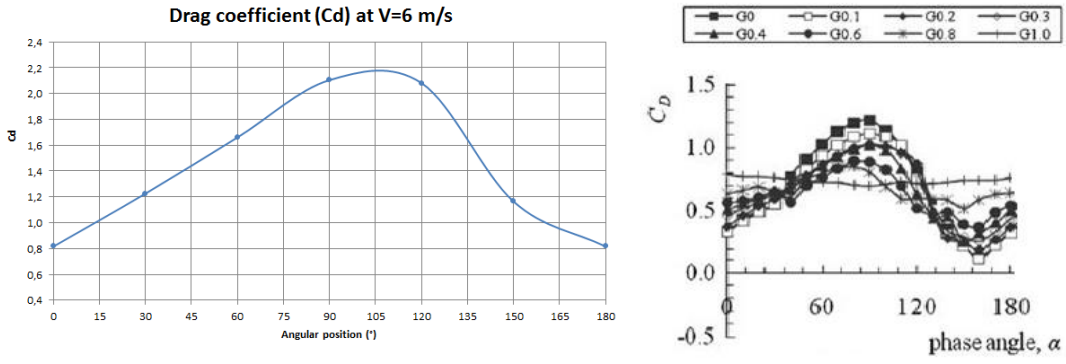

(a) (b)

Figure 68 Comparison between drag coefficients obtained in (a) this experiment and (b) Irabu and Roy [32]

In the Figure 68 it can be seen that the pattern followed by both curves is quite similar. The results in (b) show a curve with similar slopes as (a), another similarity is that all the values along the cycle are positive.

The only difference in the shape of plots that can be noted is in the last part of plot (b), between the phase angle of 160° and 180°, where there is a soft increase of C_D values.

Moreover, minimum and maximum values of (b) are very different in comparison with the ones obtained in (a). Curve in (b) shows a minimum value near 0.2 at the phase angle of 160° approximately, a value which is a bit far from the minimum drag coefficient of 0.8 obtained in (a). Maximum in (b) is about 1.0 at the phase angle near 100° whereas the maximum in (a) is about 2.2, a value much higher. But as it has been said in lift coefficients comparison, these maximums and minimums has not to be very significant because of the high values obtained at 6 m/s in Figure 64 in comparison with the rest of wind speeds tested.

Although this, almost all the differences in results above are mainly due to the different geometrical features between both Savonius rotors, because both studies have been carried out with very similar test conditions as it has been explained before.

After all these results of lift and drag coefficients analyzed it is not possible to say which one of the Savonius rotors gives better performance, because there is not a direct relation established between aerodynamic coefficients and power given by the rotor. However, the results extracted from [32] have been used to know that the aerodynamic behavior obtained in the present experiment has physical sense because of the similarity between the plots analyzed.

To sum up, after seeing the figures above, it is possible to say the Savonius wind turbine designed in this project has a similar aerodynamic behavior to the Savonius rotor analyzed in [32]. In addition, if maximum values comparisons of both coefficients are taken into account, then it can be said that the Savonius designed in this experimental study has higher aerodynamic performance.

2.3.3.6.2. Numerical study

In this section the numerical results obtained by Martorell [33] are presented. The CFD simulation has been carried out with OpenFOAM and, as it has been said before, the Savonius wind turbine simulated was exactly the same as the one designed in the present project. Moreover, test conditions were also the same in order to facilitate the comparison between both studies. The main features of this numerical study are the following:

- Turbulence model: RAS Spalart-Allmanas
- Refinement level: 14e6 cells
- Uniform air flow at 9 m/s
- No wall effects considered
- Static rotor (no rotation)

Then, numerical results provided by Martorell are shown in the Figure 69.

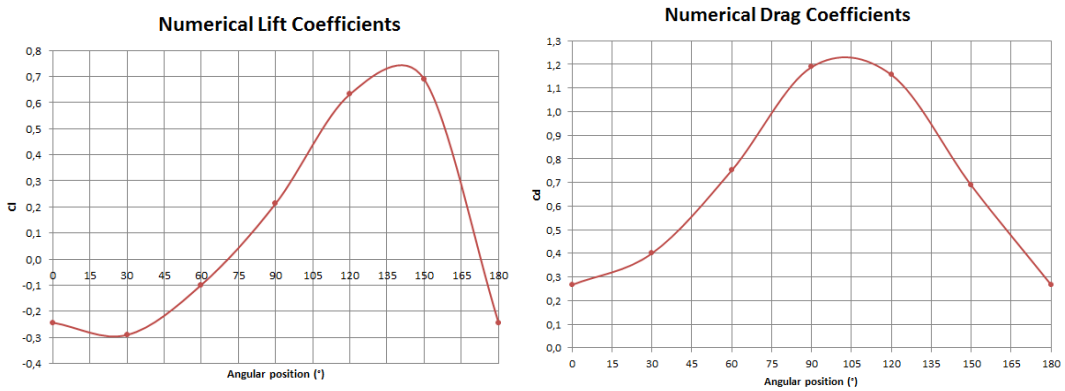

Figure 69 Numerical lift and drag coefficients versus phase angle

Comparison between the results obtained numerically and the ones obtained in this experimental study are going to be compared in the global analysis.

These numerical results plotted above are summarized in Annex II.

2.3.3.6.3. Theoretical study

Theoretical analysis of the aerodynamic performance of a Savonius wind turbine has to be carried out in order to verify the results obtained experimentally in this project.

It has to be said that only the drag analysis has been done because, in the case of lift, it is very difficult to calculate lift coefficients produced by two rotor blades theoretically. On the other hand, the computation of drag coefficients produced by two blades, one concave and another convex, is easier because they have already been calculated in many investigations and they can be found in the internet.

Thus, drag coefficient produced by the concave part of a half hollow cylinder is 2.3 and the one produced by its convex part is 1.2 as it can be seen in the Figure 70.

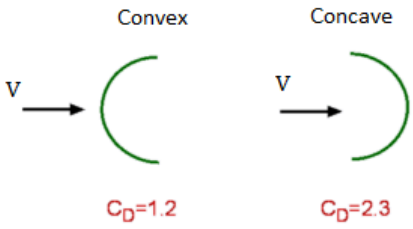

Figure 70 Drag coefficients produced by a half hollow cylinder [34]

However blades of the Savonius rotor designed in this project are not completely semi-circular, drag coefficients mentioned above are a really good approximation.

Then, some hypotheses were assumed to make the theoretical analysis of drag force.

- Incompressible flow.
- Newtonian fluid.
- Steady flow.
- Drag forces are applied at the midpoint of each blade as it is shown in the Figure 71.
- Drag coefficients remain constant regardless of angular position of the Savonius rotor.
- The twist angle of blades is very small and it is not considered.

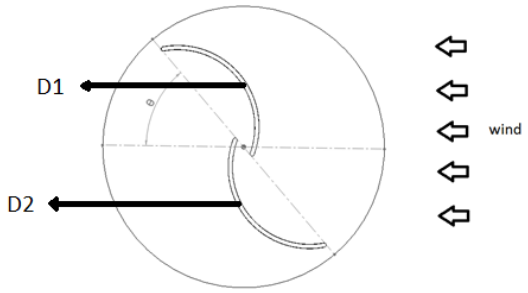

Figure 71 Scheme of drag forces on each blade of the Savonius wind turbine

Then, to calculate the total drag force the following equation was used.

$$D = \frac{1}{2}\rho A^* V^2 (C_{d1} + C_{d2}) \quad (9)$$

where C_{d1} is equal to 1.2 and C_{d2} is 2.3, ρ is the air density equal to 1.225 in (kg/m^3), V is the air speed in (m/s), and A^* is the swept area of the rotor in (m^2) and is calculated as following:

$$A^* = \frac{D}{2} \cdot H \cdot \sin\theta \quad (10)$$

where D is the diameter of the rotor in (m), H is its height in (m), and θ is the angular position of the rotor in (°). It is noted that in this case swept area takes into account the phase angle which the rotor is being analyzed.

It has to be observed that when Savonius rotor is in the 0° or 180° angular position, the swept area according to equation (10) is equal to zero, and this fact has not sense because the rotor produces drag at any angular position. Hence, it is necessary to find a different equation to compute drag force at the phase angle of 0/180°.

Thus, the following approximation can be considered. A Savonius rotor at the angular position of 0/180° has a similar shape to a cylinder placed horizontally in front of an air stream. Therefore, it can be supposed that drag coefficient produced by the rotor is the same as the cylinder which is equal to 1.17. Then, drag force is calculated as:

$$D = \frac{1}{2}\rho A^{**} V^2 C_{d.cylinder} \quad (11)$$

where A^{**} is the swept area of the cylinder in (m^2) and can be approximated as:

$$A^{**} = \frac{D}{2} \cdot H \quad (12)$$

It can be noted that, in this case, swept area of the Savonius rotor is defined as a half of the swept area defined in equation (6). This is because the projected area is significantly reduced when the rotor is positioned at the phase angle of 0/180°.

Then, when all drag forces are calculated for all angular positions and all velocities tested in the wind tunnel, they must be dimensionless so as to be compared with the results obtained experimentally.

Hence, this was done in the same way as the results obtained experimentally, using equation (7) defined in the previous sections with the swept area [A_s] calculated as (6).

Thus, the results obtained theoretically are shown in the Figure 72.

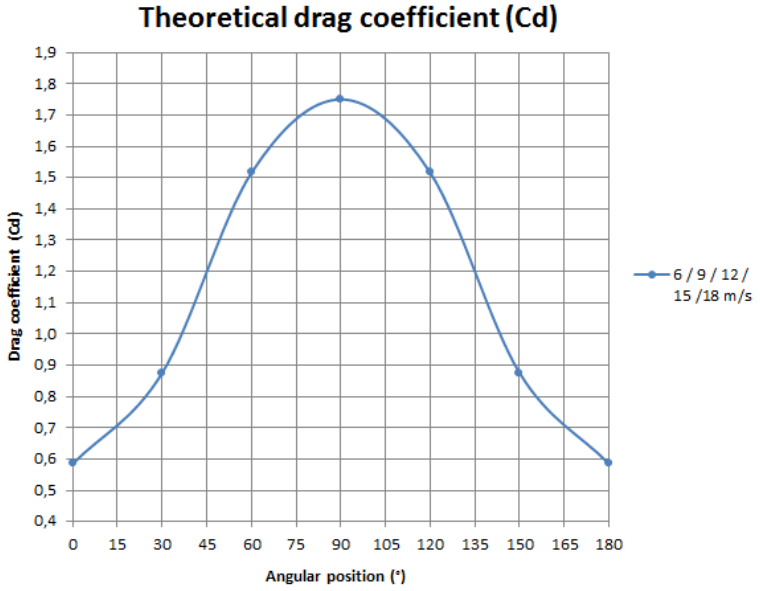

Figure 72 Theoretical drag coefficients versus phase angle

It is noted that the theoretical values of drag coefficients shown in Figure 72 do not depend on the wind speed. This means that, theoretically, the variation of Reynolds number [Re] does not affect aerodynamic coefficients of a Savonius rotor.

Full values of theoretical drag analysis can be found in Annex II.

Theoretical results obtained in Figure 72 are going to be compared with the ones obtained experimentally in experiment 1 in the next section together with numerical results.

2.3.3.6.4. Global analysis

In this section numerical and theoretical results shown above have been compared with the ones obtained experimentally in experiment 1 of this project. The three curves are plotted together in order to analyze the results in an easier way.

In the Figure 73 and Figure 74 only the results obtained at a wind speed of 9 m/s are shown. In both graphs the error associated with wind balance measurements, which was about 6-7%, has been applied on the curves obtained experimentally.

First plot contains lift coefficients obtained by the present experimental study and the ones provided numerically by Martorell [33].

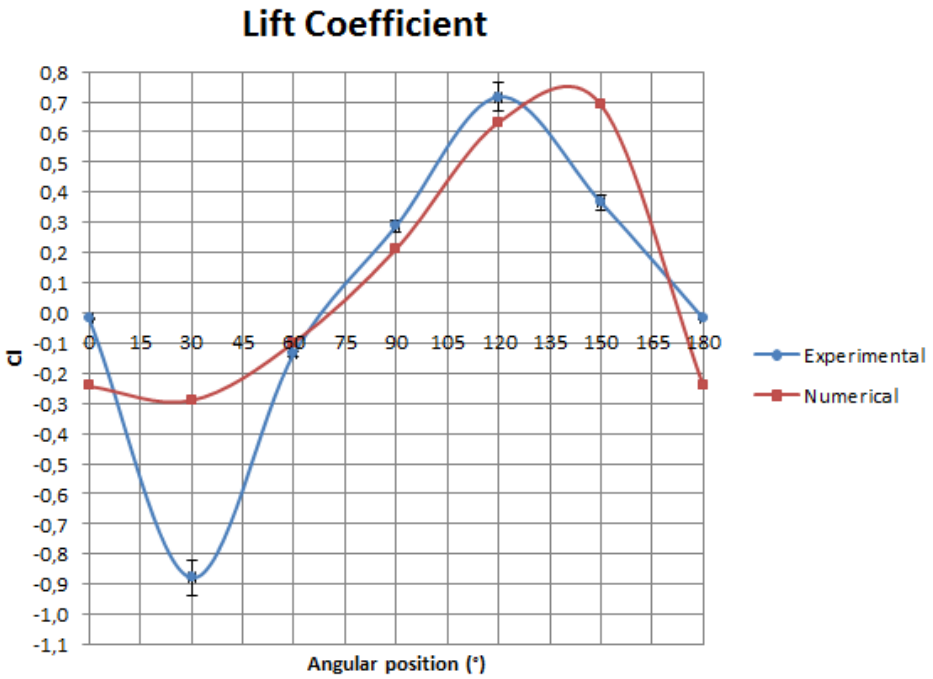

Figure 73 Global lift coefficients versus phase angle

Firstly, it is noted that curves above are quite similar, especially in the phase angle range from 60 to 180 degrees where both values are quite close.

However, in the phase angle between 0 and 60 degrees values obtained numerically are very different to the ones obtained experimentally, especially in the case of 30° where there is a difference of about 0.6 between both lift coefficients.

In the case of maximums both are near 0.75, but it can be observed that the experimental one is produced in the angular position of 120° whereas the numerical is produced at 140 degrees approximately.

These differences described are mainly due to the idealities considered in the numerical study. For instance, the simulations carried out by Martorell do not take into account

the surface roughness of the Savonius rotor. In addition, one of the hypotheses defined in the numerical study is the uniformity of the air flow, but in the experimental study carried out in the wind tunnel it is difficult to obtain a perfect uniform air flow and, therefore, some air disturbances can appear.

In the case of drag coefficients, the results provided numerically, theoretically and experimentally can be seen together in Figure 74.

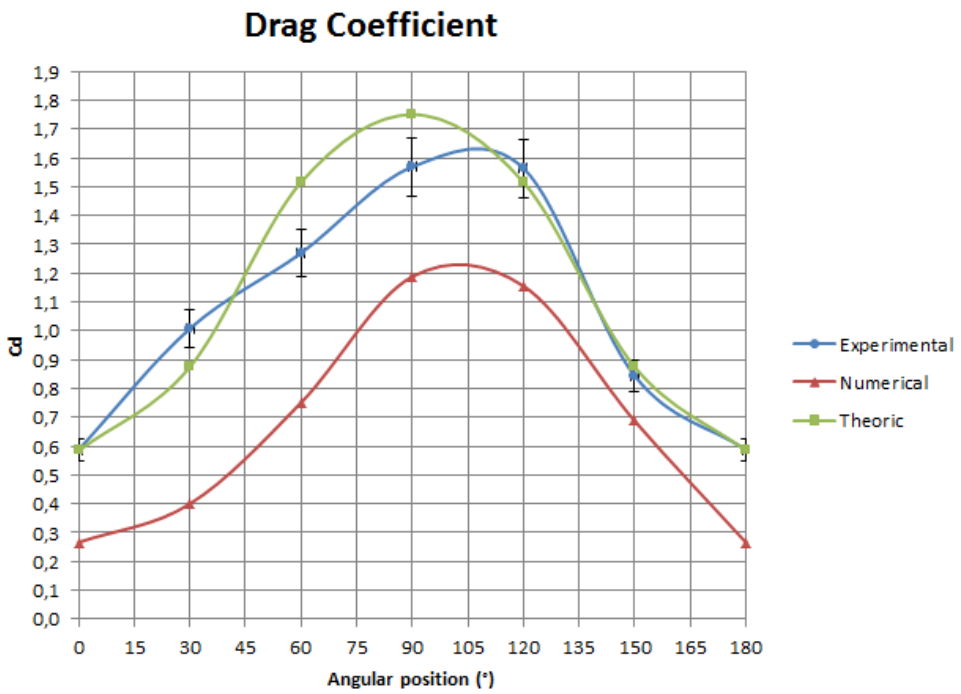

Figure 74 Global drag coefficients versus phase angle

First of all it is noted that the pattern followed by all curves are quite similar, especially between the theoretical and the experimental because they have almost the same coefficient values. It also can be observed that all the maximums are situated near the phase angle of 100 degrees and the minimum in the 0/180°.

Differences between values obtained by each study are mainly due to the following reasons. Theoretical values are higher than the rest because the same drag coefficients (2.3 for concave and 1.2 for convex) were assumed for all angular positions of rotor, which is an ideality done in order to reduce the difficulty of calculations. But logically, a half hollow cylinder will not have the same C_D when it is not placed perpendicular to the air flow.

Also other hypotheses assumed in the theoretical study, such as no twisted blades and the midpoint application of drag force, produce a loss of accuracy in the results. Although these set of idealities, theoretical results are very similar to the ones obtained experimentally in this project and, hence, it can be concluded that the theoretical study is quite good.

Now, regarding numerical results, in the plot above the effect of not considering the surface roughness of the rotor is more pronounced because part of drag force produced by the rotor is due to its roughness. Then, if it is not considered, the values obtained will be lower than the real ones, which is what can be noted in Figure 74. In addition, Martorell [33] commented in his study that the turbulence model used for simulations (RAS Spalart-Allmanas) gives lower drag coefficients than the real ones.

In general, it can be concluded that the experimental results of C_L and C_D obtained in this experiment 1 are satisfactory.

2.3.4. Experiment 2: Static torque

The purpose of this experiment is to obtain static torque coefficients of the Savonius wind turbine for different phase angle positions. These angular positions analyzed are the same as the ones studied in the previous experiment: 0, 30, 60, 90, 120 and 150 degrees, taking into account the periodicity of results every 180 degrees due to the symmetry of the rotor.

In this case, wind speeds used to test the Savonius rotor were 6, 7, 8, 9, 10, 11 and 12 m/s. This range of velocities is shorter than the one used in experiment 1 because the Savonius wind turbine usually operates at low wind speeds and, hence, it is interesting to obtain the static torque at low air velocities.

The facilities used to carry out the present experiment were the wind tunnel of the Fluid Mechanics Department described before and its test bench.

The equipment used to measure static torque produced by the Savonius rotor is described in the following section.

2.3.4.1. Torque sensor

The torque sensor was a Lorenz DR 2112 as it can be seen in the Figure 75. It can measure a maximum torque of 5 Nm. Therefore, taking into account that a Savonius rotor produces low torque, it is noted that this sensor has a full scale too big. However, it was used because there was no other option available.

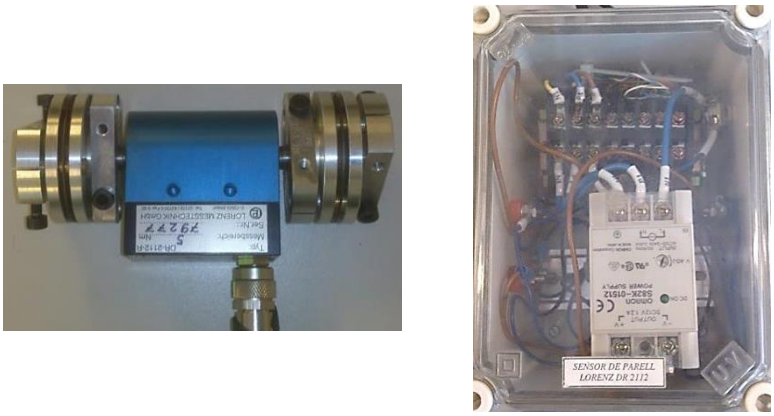

Figure 75 Lorenz DR 2112 torque sensor

In Figure 75, image on the left is the torque sensor and image on the right is the junction box which contains all electrical connexions needed to process the measurements of the sensor. Logically, both elements are connected between them via cable. It is necessary to say that this connection is really important due to its sensitivity, especially in the junction between it and the torque sensor because any abrupt movement of this cable can disturb the torque measurements.

Before carrying out tests, it was very important to make an exhaustive revision of this sensor because of the amount of years that it had not been used. First of all, it was necessary to read all the necessary documentation about it in order to understand its performance. The next step was to make a full inspection of the system so as to check all the connections and, in this way, prepare the sensor for being used in the experiment.

For instance, a copper wire situated inside the cable which connects the sensor with the junction box was repaired and welded.

But in addition, before the final experiment in the wind tunnel, a preliminary test was necessary to be made to check the good performance of the sensor. The test was made as it is shown in the Figure 76.

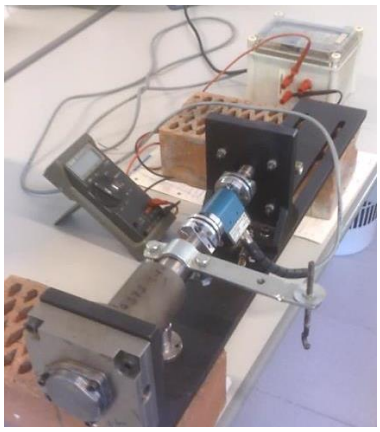

Figure 76 Test carried out to check the performance of torque sensor

In Figure 76, three main elements can be observed. The first one, in the middle of the image the torque sensor attached to a metal shaft structure. At the top it is noted the junction box described previously and, finally, on the left it is observed a multimeter which is the interface used to know the torque measured by the sensor. This multimeter is connected to the junction box .

The test consisted in hanging some weights from the horizontal metal bar through the hook that can be seen in the figure above. Then, knowing the mass of different weights and the distance between the hook and the metal shaft where torque sensor is attached, it is possible to calculate the theoretical torque produced by weights.

To make a valid calculation, it is important to ensure the perpendicularity between the horizontal arm where the weight is hanged and the metal shaft. A more detailed view of these elements is shown in the Figure 77.

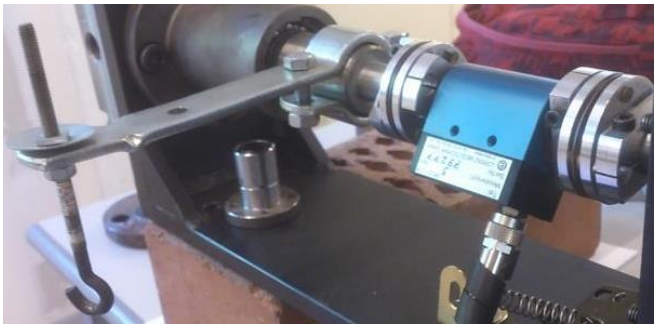

Figure 77 Detailed view of horizontal arm, hook and torque sensor attached to the metal shaft

Thus, if the theoretical torque calculated and the experimental torque measured by the sensor agree, it means that the torque sensor is well-calibrated and is ready to be used.

The scale of multimeter for torque measurements is the following:

$$1\,V = 1\,Nm$$

Hence, the multimeter gives directly the torque measured by the sensor. It has to be said that an approximate error of about 0.5% of full scale must be considered in the measurements of torque sensor.

2.3.4.2. Support structure

As a support structure, a metal structure provided by the technician Jaume Bonastre of Fluid Mechanics Department was used. This structure had been used to measure torque of a metallic wind turbine in the wind tunnel many years ago. Hence, it was very suitable for this experiment.

The structure only had one drawback, it had been used to test a heavier and bigger wind turbine than the one designed in this project, which is made of ABS plastic. Hence, the whole structure, including the metal shaft and bearings, was oversized for the present case.

It is important to take into account this oversizing described because it will induce a small torque against rotation of the Savonius rotor, producing that at low speeds the rotor does not rotate. Luckily, in this experiment it is not necessary the rotation of Savonius rotor because, as the title of experiment says, the rotor is static during the measurements. Although this, oil was added to bearings so as to reduce friction.

A view of the support structure with Savonius rotor and torque sensor attached can be observed in the Figure 78.

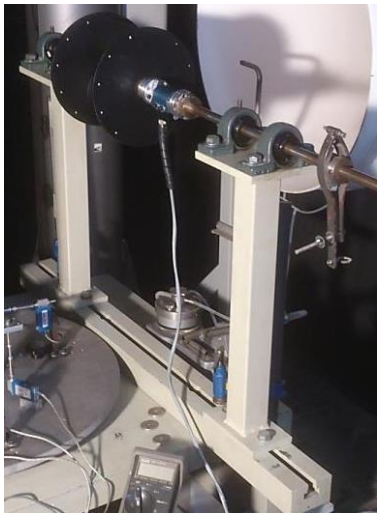

Figure 78 Support structure used to carry out the experiment 2

The structure in grey is the support structure used. It is made up of a horizontal bar which has a linear hole along its longitude where two metal columns can be moved through. At the top of each column there are two black bearings. It also can be noted the rusty metal shaft.

2.3.4.3. Assembly and procedure

The most complicated part of this experiment was to attach the Savonius rotor, the torque sensor and the metal shaft together because each element had a different diameter.

The first option was to make the necessary coupling pieces with a 3D printer, but it was firmly discarded because of the high price of printings. Then, the second option was to make couplings with a lathe situated in Fluid Mechanics Department. This option was the fastest and cheapest one.

Hence, with the help of the technician Justo Zoyo, some coupling pieces were made taking into account the position of each on the final assembly and the elements they have to attach. An example of a coupling piece is shown in the Figure 79.

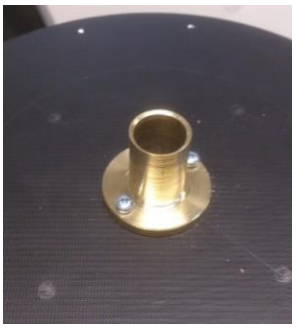

Figure 79 Coupling piece of the Savonius rotor with the shaft of support structure

As it is noted, the pieces were metallic with a yellow tone. Thus, only 3 coupling pieces were made and the final assembly of all them with the other components can be observed in the Figure 80.

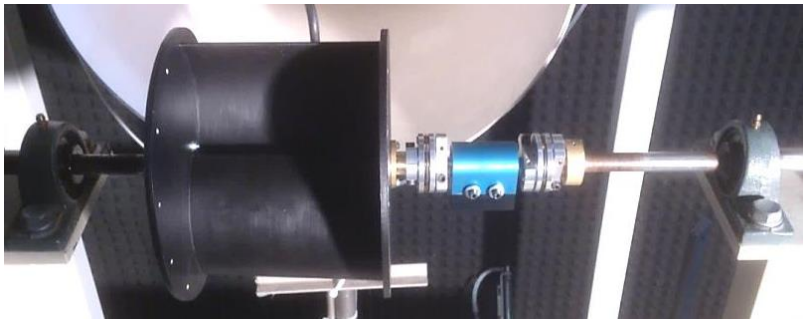

Figure 80 Assembly of all the elements with coupling pieces

In Figure 80 the rotor has a coupling piece on each of its sides, and the same occurs with the torque sensor. Both elements share one coupling piece which is situated in the middle of them.

The one on the left attaches the metal shaft with the left end plate of the Savonius rotor. This coupling piece was like the one shown in Figure 79, which in one extreme there is a hole of 15 mm of diameter to attach the shaft and the other extreme is screwed to the rotor end plate with screws of metric 3, adding nuts and packing rings. On the other hand, the metal shaft was fixed to the coupling piece with studs of metric 3. Holes for screws were made with the vertical drill situated in the Fluid Mechanics laboratory, it was necessary to take care not to damage rotor blades during the drilling of the end plate.

The central coupling piece which attaches the right end plate of the rotor and the left part of the torque sensor was similar to the one described above. The part attached to the rotor end plate is fixed with screws in the same way as the other, but the extreme attached to the torque sensor is a cylinder of 18 mm of diameter which is introduced

inside the sensor. This cylinder is fixed to the sensor with an own tightening system of the sensor.

The third coupling piece which attaches the right part of the sensor and the shaft is a bit different. The extreme attached to the sensor is fixed in the same way as the last coupling piece described, with a cylinder of 18 mm of diameter. The other extreme has a hole of 15 mm of diameter where the metal shaft is introduced and fixed by studs of metric 3.

It has to be said that the two metallic columns of the support structure can be moved horizontally in order to strengthen the structure and make more rigid all coupling joints.

In this experiment, the wind tunnel operates in the same way as experiment 1. It is controlled by the control device which allows controlling the wind speed. Moreover, wind speed is measured by the same manometer and pitot static probe as the first experiment. Then, once all the elements and components of the equipment are described, the following scheme can be made in order to have a clearer view of the present experiment (Figure 81).

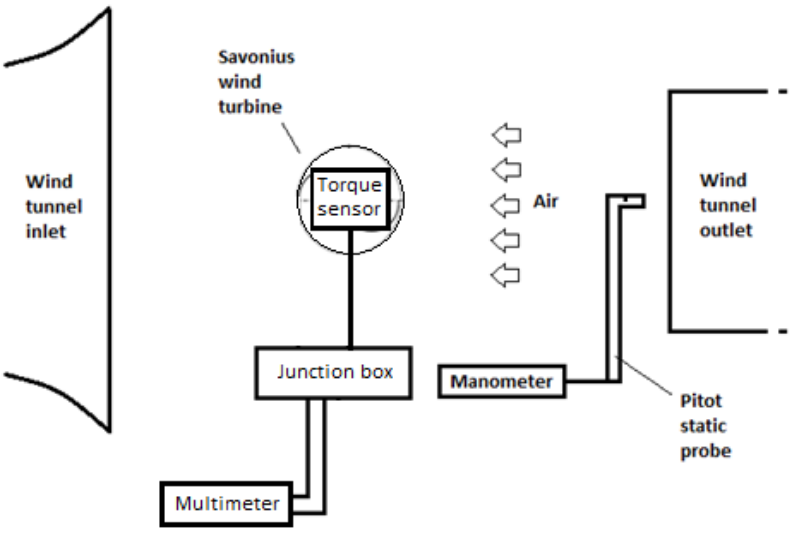

Figure 81 Schematic diagram of experiment setup

Junction box must be connected to electric system to have the torque sensor operative. It also has to be said that the base of the support structure was fixed to the table which was over with locking devices in order to avoid possible vibrations or swings of the whole structure. In addition, the height of the metallic columns of the support structure was suitable because they sustain the rotor exactly at the same level as the center of the wind tunnel outlet.

Hence, after seeing a scheme of the experiment, the real final setup in the test bench of wind tunnel is shown in the Figure 82.

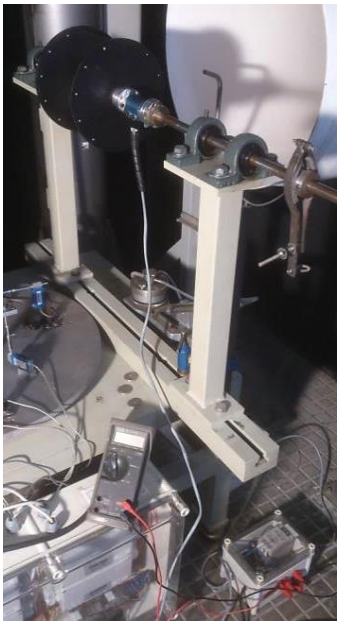

Figure 82 Experiment setup

It is noted the support structure with the Savonius rotor and torque sensor both attached to the shaft. At the bottom of the image there are the junction box and the multimeter with all connections ready to be used.

As some velocities used in this experiment are different from the ones used in experiment 1, the lengths of alcohol column corresponding to these velocities (Table 8) have to be calculated with equations (3) and (4) defined previously.

V [m/s]	V [km/h]	l [mm]
6	*21.6*	**5.7**
7	*25.2*	**7.8**
8	*28.8*	**10.2**
9	*32.4*	**12.9**
10	*36*	**15.9**
11	*39.6*	**19.2**
12	*43.2*	**22.9**

Table 8 Relation between the test speeds and its corresponding length of the alcohol column

Once all air velocities are defined, the first step in order to carry out the tests was to turn on the multimeter, the torque sensor and the wind tunnel. Then, the next step is to modify wind speed turning the power regulator until a desired velocity.

Thus, fixing the rotor angular position holding the shaft with the hand it is possible to obtain all necessary static torques produced by the rotor for each phase angle and wind speed.

In order to fix the angular position of the rotor, apart from holding the shaft, the holes made in experiment 1 to fix the phase angle of the Savonius rotor were used to have a clear reference of which angular position was being tested. The only thing it was necessary to be done is to maintain the hole which is being tested at the same height of the shaft. A clear view of holes is shown in the Figure 83.

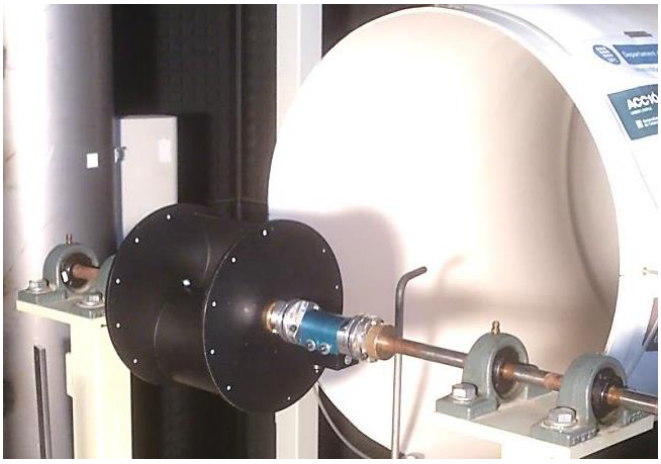

Figure 83 View of holes of the rotor end plates used as reference to know the phase angle

It is necessary to remember that the torque sensor gives static torque in (Nm), but in order to study and analyse the results they must be dimensionless. Therefore, the static torque coefficient must be calculated.

Static torque coefficient (C_{Ts}) is calculated with the following equation:

$$C_{Ts} = \frac{4T}{\rho V^2 A_s D} \tag{13}$$

where T is torque given by the torque sensor in (Nm), ρ is air density in (kg/m^3), V is air speed in (m/s), A_s is the swept area in (m^2) defined as the equation (6) and, finally, D which is the rotor diameter in (m).

Thus, the results obtained are presented in the following section.

2.3.4.4. Results

Firstly, it is necessary to say that all the results obtained from experiment 2 are in Annex II. Then, static torque coefficients obtained in this experiment are shown in the Figure 84.

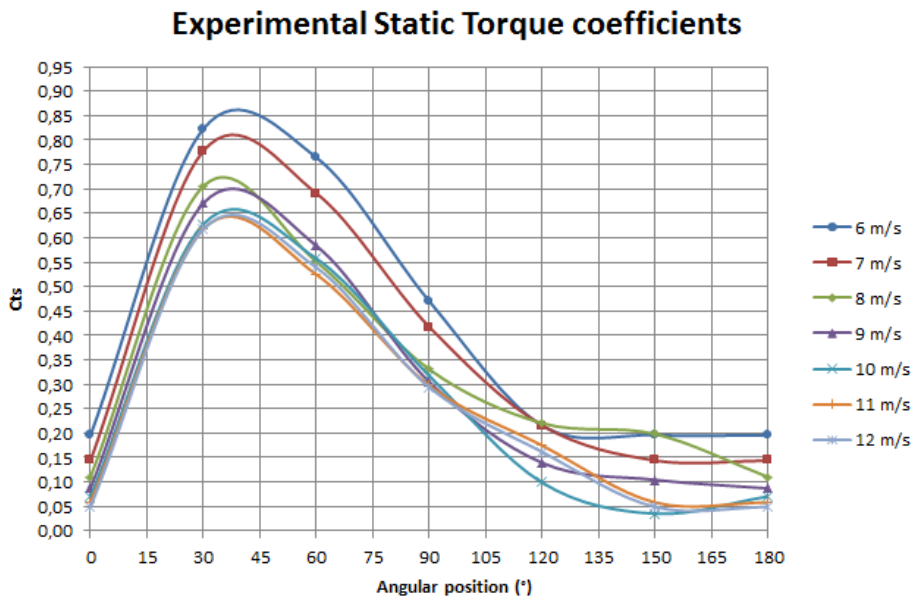

Figure 84 Static torque coefficients versus phase angle

In Figure 84 it can be seen the curves of results obtained in the measurement of static torque of the Savonius rotor designed in the present study. It is noted that all curves follow the same pattern, a first increase in the phase angle range from 0 to 35 degrees approximately until the maximum, which can be situated in the angular position of about 35-40°. Then, a linear decrease from 40 to 135 and, finally, values remain constant until the phase angle of 180°.

This pattern followed by all curves seems to be correct because as the phase angle is increasing, more blade surface is in contact with the air flow producing an increase of the forces on each blade which, logically, are higher in the concave part than in the convex one. This difference of forces on each blade produces a torque about shaft. As rotor continues increasing its phase angle, this difference of forces mentioned becomes smaller and, hence, static torque produced decreases too.

It is interesting the fact that all maximums are clearly situated in the phase angle of 35-40°. All curves are very close to each other, especially the ones obtained at the wind velocities of 8, 9, 10, 11 and 12 m/s. The other two, which are the cases tested at 6 and 7 m/s, have higher values in almost all phase angle range. This fact also has been observed in experiment 1, where values of lift and drag coefficients at 6 m/s had higher values than the rest of tests.

The maximum value of static torque coefficient obtained is near 0.86 at the wind speed of 6 m/s. The rest of maximums are around 0.65 and 0.70. In the case of minimums, they are all between 0.05 and 0.2.

It has to be noted that all static torque coefficients obtained experimentally are positive, there is no range of negative values.

2.3.4.5. Experimental results comparison

As it has been done with experiment 1 about aerodynamic forces, experimental results obtained by torque tests carried out in the Fluid Mechanics Department are going to be compared in three different ways:

- Two experimental studies of static torque over a Savonius wind turbine carried out by Irabu and Roy [6] and Kamoji et al. [20].
- Numerical study with CFD of static torque over a Savonius wind turbine carried out by Martorell [33].
- Theoretical study of static torque over a Savonius wind turbine.

Both experimental studies mentioned above have been carried out with similar Savonius rotors as the one designed in the present study. Geometrical parameters of both rotors are summarized in the Table 9 and Table 10 respectively.

Feature	Value
Number of blades	**2**
Number of stages	**1**
Aspect ratio (AR)*	**1.78**
Overlap ratio (β)*	**0.14**
Twist (α)*	**0°**
Blade arc angle (ψ)*	**180°**
Shaft	**Yes**
End plates	**Yes**

Feature	Identifier	Value (mm)
Rotor height	*H**	**160.00**
Rotor diameter	*D**	**89.89**
End plates diameter	D_f*	**160.00**
Shaft diameter	d_{shaft}*	**3.00**
Blades diameter	*d**	**90.00**
Overlap distance	*e**	**15.6**

Table 9 Geometric features of the Savonius rotor used by Irabu and Roy [6]

Feature	Value
Number of blades	**2**
Number of stages	**1**
*Aspect ratio (AR**)*	**0.77**
*Overlap ratio (β**)*	**0.10**
*Twist (α**)*	**0°**
*Blade arc angle (ψ**)*	**124°**
Shaft	**No**
End plates	**Yes**

Feature	Identifier	Value (mm)
Rotor height	*H***	**-**
Rotor diameter	*D***	**-**
End plates parameter	D_f^{**}/D^{**}	**1.1**
Shaft diameter	d_{shaft}**	**-**
Blades diameter	*d***	**-**
Overlap distance	*e***	**15.6**

Table 10 Geometric features of the Savonius rotor used by Kamoji et al. [20]

The experimental study carried out by Irabu and Roy had the Savonius rotor positioned vertically in front of the air flow and tests were made at an air speed of 6 and 9 m/s.

In the case of the study carried out by Kamoji et al. the rotor was placed vertically too and the wind speed was about 8.35 m/s.

This small difference between air velocities in both studies above is not going to be a problem when comparing the results because, as it has been possible to see in experimental results shown in Figure 84, static torque does not change so much for different air speeds.

In the case of the numerical study carried out by Martorell [33], the Savonius tested has exactly the same geometry as the rotor used in this project and, in addition, numerical simulations were made with the same test conditions as the ones used in the laboratory. Hence, there is not going to be any drawback in the analysis and comparison of both results.

In the theoretical study, Savonius rotor of this project is going to be analyzed so as to compute static torque coefficients theoretically.

2.3.4.5.1. Experimental studies comparison

In this section the results obtained in the present experiment, C_{Ts}, are going to be analyzed in comparison with results obtained by Irabu and Roy [6] and Kamoji et al. [20].

Static torque coefficients extracted from both experimental studies are defined with the same equation as the one used in the present project, equation (13), with the same swept area definition. Both results are presented in the Figure 85 and Figure 86.

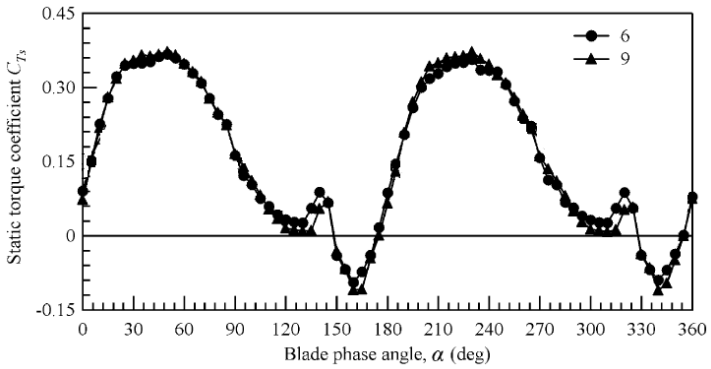

Figure 85 Static torque coefficient versus phase angle by Irabu and Roy [6]

It is noted that the results obtained at 6 and 9 m/s have no difference between them in curves shown in Figure 85. In addition, measurements were done every 5 degrees of the phase angle of rotor. This is the reason of why so many points can be observed in the plot.

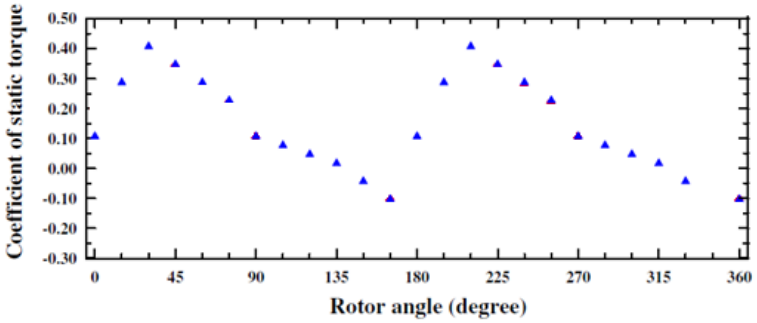

Figure 86 Static torque coefficient versus phase angle by Kamoji et al. [20]

The results plotted in Figure 86 do not have as many points as the graphic in Figure 85. However, the shape or pattern followed by the results can be observed easily too.

Thus, the plot of static torque coefficients at 9 m/s obtained in the present project is shown below in order to be analyzed in comparison with both figures above. Wind velocity of 9 m/s is chosen because is the closest speed to the ones used in the experimental studies that are being compared.

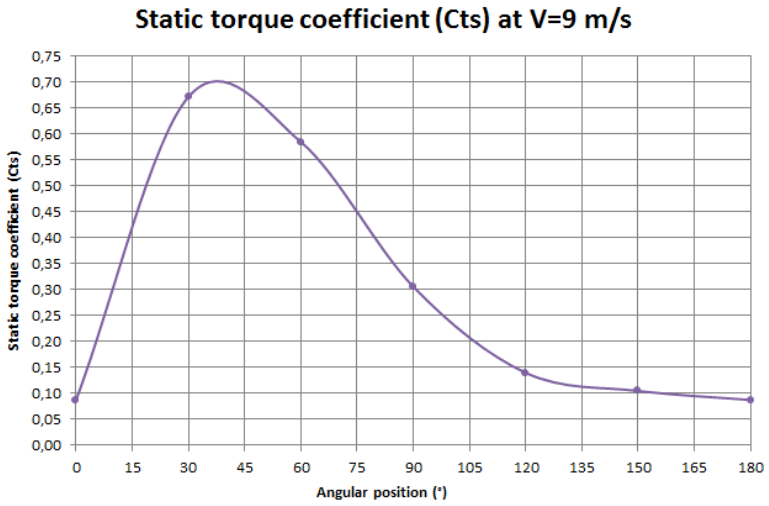

Figure 87 Static torque coefficients obtained in this study versus phase angle

It has to be observed that the Figure 87 has the phase angle plotted from 0 to 180° due to the symmetry of results each 180 degrees. This periodicity can be noted in Figure 85 and Figure 86 where two periods of 180° can be clearly distinguished. Hence, only the first period of each figure is going to be analyzed in the following paragraphs.

If the three figures above are compared, it can be observed that curves have many similarities. For instance, the maximum static torque coefficient of each graphic is situated in the phase angle of 35-40 degrees approximately, also that the pattern followed by results of each study is very similar, with very few differences.

These differences are mainly two. The first one is the maximum static torque values, which in the case of two experimental studies that are being compared they have their maximums near 0.4. On the other hand, in the case of the present study the maximum static torque coefficient is about 0.70, a rather higher value.

The other difference can be observed in the phase angle range from 150 to 180 degrees, where in the case of this study C_{TS} obtained in this range are clearly positive, whereas the ones obtained by the other two experimental studies are negative.

This is an important feature to be taken into account because it is an advantage over the other rotors. This feature means that the Savonius designed in this project has better static torque performance than the rotors analyzed by Irabu and Roy and Kamoji et al. in their respective researches.

These differences in the results commented above are clearly due to different geometrical configurations of each Savonius rotor used on each study, because the other test conditions are very similar between all three experimental studies compared.

In conclusion, after the analysis of results carried out in this section, it is possible to say that the Savonius wind turbine designed in this project has better starting torque

characteristics than rotors used by Irabu and Roy [6] and Kamoji et al. [20] in their studies.

2.3.4.5.2. Numerical study

In this section the numerical results of static torque coefficients provided by Martorell [33] are presented. Regarding simulations, hypotheses defined in experiment 1 are also valid for this case. It is necessary to remember that simulations were carried out at a wind speed of 9 m/s.

Then, numerical results provided by Martorell are shown in the Figure 88.

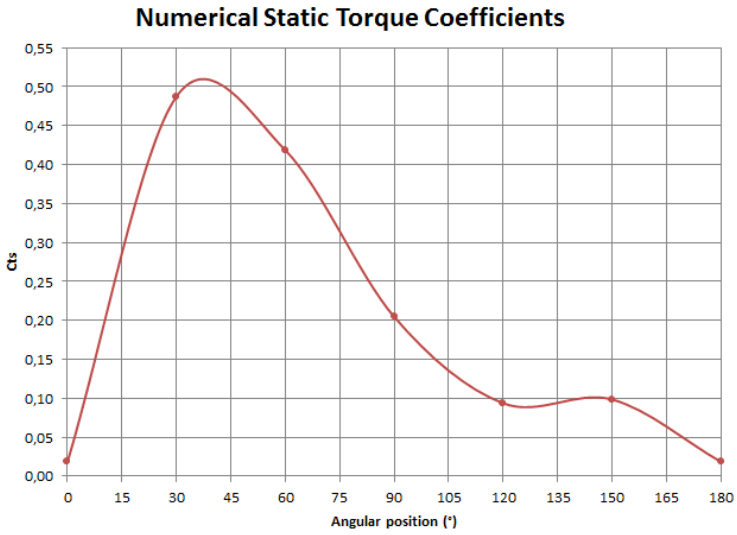

Figure 88 Numerical static torque coefficients versus phase angle

The comparison between results obtained numerically and the ones obtained in this experimental study are going to be compared in global analysis.

2.3.4.5.3. Theoretical study

The theoretical analysis of static torque of a Savonius wind turbine has to be carried out in order to verify the results obtained experimentally in this study.

This theoretical study is done under the same hypotheses described in the theoretical study of aerodynamic forces.

Moreover, this analysis is going to use the equations defined in that case in order to calculate static torque and its coefficients. Because the static torque produced by a Savonius rotor depends on drag forces over each blade.

Hence, to compute the static torque theoretically, the Figure 89 must be shown.

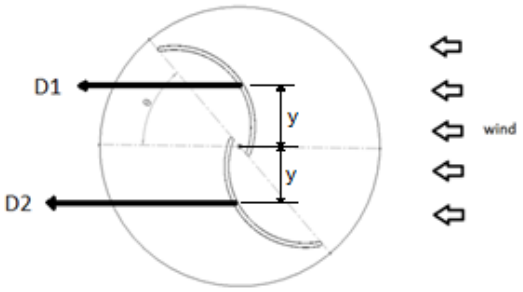

Figure 89 Scheme of drag forces on each blade and their lever arm

To calculate static torque it is necessary to do the subtraction between the two drag forces multiplied for their respective lever arms to the rotor axis, which are equal and are named *y* according to the figure above. They can be computed as following:

$$y = \frac{D}{4}\, sin\theta \tag{14}$$

where *D* is the diameter of the rotor in (m) and θ is the angular position in (degrees) that is being tested.

Then, taking into account the equation (9) which describes the drag force on each blade. Static torque can be calculated with the following equation.

$$T = y\frac{1}{2}\rho A^{*}V^{2}(C_{d2} - C_{d1}) \tag{15}$$

where *T* is the static torque in (Nm) and A^{*} is defined as the equation (10) described in the theoretical study of experiment 1.

In this case the drag force produced by the Savonius rotor at the angular position of 0/180° is not going to be taken into account because the torque given is almost zero. Therefore, the torque given at this phase angle is considered zero directly.

It has to be said that static torques obtained theoretically has to be dimensionless to be compared with other static torque results. In order to do so, the equation (13) has been used.

Finally, static torque coefficients obtained theoretically in this section are shown in the Figure 90.

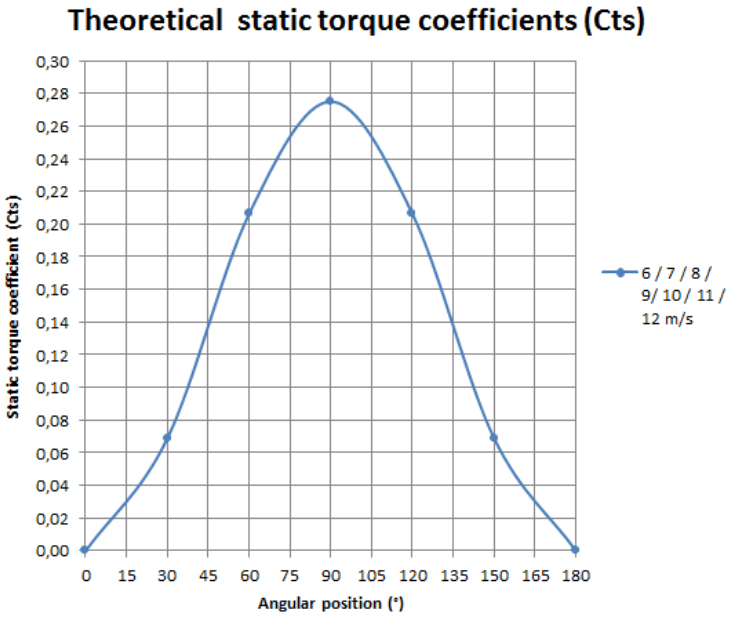

Figure 90 Theoretical static torque coefficients versus phase angle

It is noted that the theoretical values of static torque coefficients shown above do not depend on wind speed. This means that the variation of Reynolds number [Re] does not have effect on static toque coefficients of a Savonius rotor.

All values of the theoretical static torque study can be found in Annex II.

Theoretical results shown in Figure 90 are going to be compared with the ones obtained experimentally in experiment 2 together with simulated results.

2.3.4.5.4. Global analysis

In this section numerical and theoretical results analyzed above have been compared with the ones obtained experimentally in the present experiment 2. All three curves are plotted together in order to analyze the results in an easier way.

In the experimental results plotted below, the error considered in the measurements provided by torque sensor, which was about 0.5% of full scale, has been applied on the curve.

In the Figure 91 only the results obtained at a wind speed of 9 m/s are shown. Thus, static torque coefficients of each study are the following:

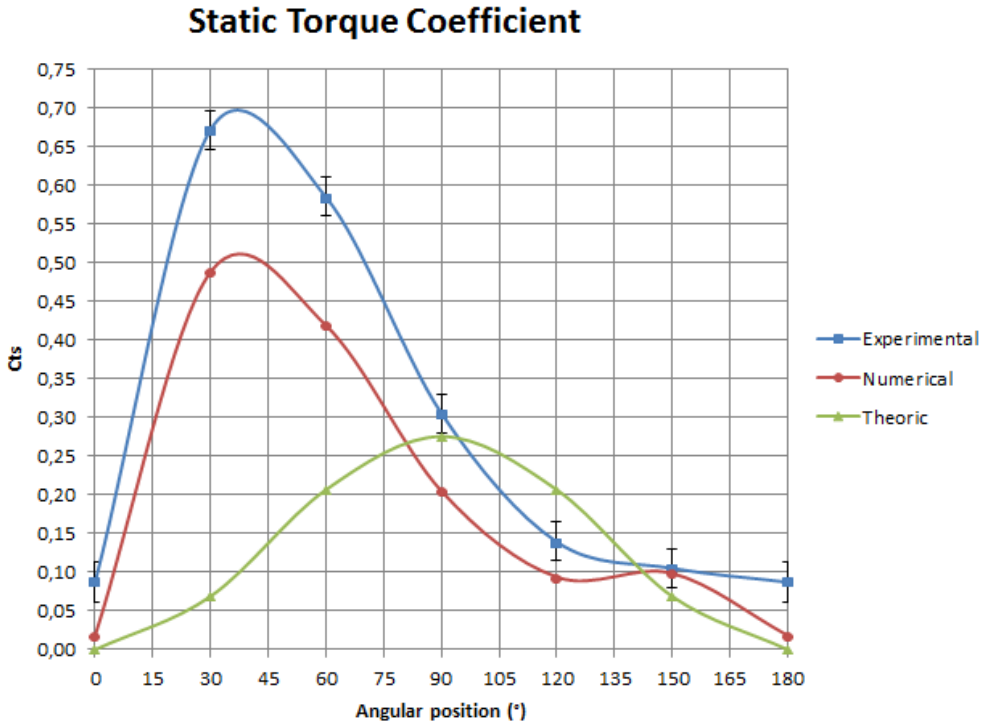

Figure 91 Global static torque coefficients versus phase angle

In Figure 91 it is possible to see that there exists a huge difference between experimental and numerical studies regarding theoretical one.

Results obtained experimentally and numerically follow similar curves with almost the same pattern. But in the case of theoretical results, they follow a curve quite different from the rest mainly in the phase angle range from 0 to 90°, because after this angular range the margin of difference is greatly reduced.

This great difference in the first half of the plot above is due to hypotheses assumed in the theoretical study of static torque coefficients. According to this study, static torque is calculated with the subtraction of torque produced by the drag force of each blade about rotor axis. As it has been said before, drag coefficients for these two forces were defined as constant at any phase angle of the rotor. This approximation has not had a huge effect in theoretical drag coefficients calculated in experiment 1, but in this case it is noted that this approximation cannot be assumed because of the discrepancy on the results shown in the previous figure.

Another reason of these huge differences related to theoretical results is that the theoretical study done does not take into account the positive torque effect produced by the overlap distance of the rotor, which is a very important parameter for torque performance.

Therefore, the theoretical study should be improved in order to acquire more accurate results.

Regarding results obtained experimentally and numerically, reasons of the little difference between both curves is the same as the ones explained before in the case of C_L and C_D, which refer to hypotheses assumed in the simulations carried out in numerical study.

These hypotheses, especially the no consideration of surface roughness, have a great effect in numerical drag coefficients as it has been possible to see in Figure 74. Hence, static torque coefficients will also suffer the effects of these hypotheses due to its direct relation with C_D.

In addition, as it has been explained in the global comparison of drag coefficients before, Martorell [33] commented in his numerical study that the turbulence model used for simulations (RAS Spalart-Allmanas) gives lower drag coefficients and, therefore, lower C_{Ts}.

Although these little differences, in general the results obtained numerically and experimentally are satisfactory because of the great similarity between them. In the case of theoretical results, they should be calculated in a more accurate way so as to get values more similar to experimental ones.

Chapter 3

3. Fulfillment of the scope and specifications

All tasks described in the scope have been achieved. Firstly, the exhaustive bibliography research was done in order to start the theoretical and geometrical study of Savonius wind turbines. All conclusions extracted from this theoretical and geometrical study were used to select the most important properties of the Savonius rotor that was being designed, such as number of blades, overlap ratio and aspect ratio among others. These main characteristics defined the necessary geometry of rotor so as to build the 3D model.

Once 3D model was ready, the next step was to print it by a 3D printer as soon as possible to begin experiments. But after tests, it was needed to treat the Savonius rotor surface in order to adequate it to aerodynamic purposes of the project.

Then, the necessary material and equipment to carry out experiments was prepared and assembled to facilities in the laboratory with adequate instruments. It has to be said that this part was the most difficult and longer due to the amount of problems that had to be faced. However, tests were developed and the necessary measurements were achieved.

The post treatment of results was carried out satisfactorily during the last days of project and, finally, the conclusions and recommendations presented in this work were written.

Chapter 4

4. Environmental impact

As it has been seen in the present report, this project has a theoretical and an experimental part. The experimental block is longer than the theoretical one, hence, it is logic to think that the main environmental impact is produced by experimental tests. However, some environmental aspects about theoretical part will be analyzed too.

It must be said that one of the justifications of this project was the fact that renewable energies were growing and also that wind energy was becoming a very important source of clean energy in the world. Therefore, it was necessary to carry out a study of a Savonius wind turbine in order to obtain some significant results about its performance. The Savonius rotor geometry was defined according to the results and conclusions extracted from all the bibliography researched so as to design a more efficient rotor.

Hence, the rotor designed in the present study should provide more power and, thus, more clean energy than a Savonius rotor with a standard geometry. This improvement in rotor performance should reduce the energy consumption of non-renewable sources and, in this way, reduce the pollution of the earth.

However, in this project have been used some devices which consumed a great amount of energy during their performances, such as the wind tunnel, the 3D printer and the 3D removal system.

The first one, despite not working with fuel, wind tunnel consumes a lot of energy because of its powerful electric motor. The approximated power consumed is about 30 hp (22065 W). It also must be noted the acoustic pollution that it produces.

Next device is the 3D printer, which needed a great amount of energy and hours to print the Savonius rotor designed in this project. It consumes about 1380 W and it needed 25 hours to print the whole rotor. Moreover, 3D printer used had heat emissions of 2550 BTU/hour, which is equivalent to 747.3 W. Finally, the acoustic pollution produced by it was about 62 dB during the printing, which is a value of dB that should be a bit annoying to human hearing.

The 3D removal system is similar to the 3D printer described above. It consumes about 1200 W of energy during its performance and, in this case, there is no information about heat emissions and its acoustic pollution. It has to be taken into account that this device needed 12 hours to remove the additional material of the Savonius rotor printed.

It is also interesting to analyze the energy consumed by the laptop used to develop this project. The laptop was used to write all the necessary documentation such as the report, and it was also used to carry out other activities such as 3D modeling of the rotor and post processing of the results. The average of energy consumption of it was about 20 W during the whole study.

To sum up all the energy consumed in this project, the following Table 11 is made. It must be said that is an approximation.

Device/Item	Hours (h)	Energy consumption (kWh)	CO_2 emissions (kg of CO_2)
Wind tunnel	5	110.32	71.71
3D printer	25	34.50	22.42
3D printer heat emissions	25	18.68	12.14
3D removal system	12	14.40	9.36
Laptop HP Pavilion dv6	356	7.12	4.63
TOTAL			**120.26**

Table 11 Equivalent CO2 emissions from energy consumption during this project

It has to be said that once this study has finished, the Savonius rotor designed can be reused for future academic purposes in the laboratory of Fluid Mechanics Department. In this way, the rotor has not to be necessarily recycled and can have a longer life cycle.

Chapter 5

5. Safety and social considerations

Regarding the safety aspects of this project, facilities and machines used in the Fluid Mechanics Department have some safety recommendations or obligations that must be followed in order to prevent any damage in the assistant.

In the usage of wind tunnel, it should be compulsory to use headphones or earplugs so as to prevent ear damages as sound produced by the wind tunnel motor is continuous and could have a harmful effect. Moreover, the model tested in its test section must be appropriately fixed to the test bench to avoid possible escapes because of the heavy wind. In the hypothetical case that it flies off, a grill is situated in the nozzle to prevent possible accidents. It also is very important to turn off the wind tunnel while test model is being manipulated in the test bench.

Moreover, some safety conditions must be followed during the performance of the vertical drill and the lathe. These machines are mainly used to perforate elements, in this case they have been used to drill the Savonius rotor made of ABS plastic and some metallic pieces. During their performances, goggles must be used to protect the eyes from metallic shavings that can fly out. In addition, it is essential to ensure that bits are correctly fixed in order to avoid fatal accidents. For this reason, protective gloves must be used.

The most remarkable social aspect is that this study could be a laboratory practice in the future. Because this project contains both theoretical and experimental parts which can be perfectly understood following the present report. In addition, the assembly and usage of all the necessary components to carry out tests are described in detail in order to achieve the best performance of instruments and model tested.

Moreover, tests done in the present project, such as the aerodynamic study in the wind tunnel, are closely related to the matter covered in Fluid Mechanics subject. Thus, this project could be a different way for students to understand and apply the theory bases of the subject experimentally.

Chapter 6

6. Scheduling of the project

In an experimental study it is essential to allow experiments to be flexible in terms of availability of facilities and also in terms of calendar compatibility with the director or co-director of the study, as they are a source of information and knowledge that support you during the whole cycle of the project.

6.1. Planning of the project

1. Theoretical and geometrical study

    a. State of art of investigations about Savonius wind turbines in scientific databases.
    b. Study of different geometric characteristics of a Savonius rotor according to the bibliography researched previously.
    c. Analyze results obtained by the others researchers from their investigations.
    d. Conclude what is the best geometrical configuration of a Savonius rotor for the present experimental study.

2. Savonius rotor design

    a. Summarize the geometrical features selected from previous theoretical and geometrical study.
    b. Calculation of all the necessary measures of the rotor according to geometrical parameters chosen previously.
    c. Building the 3D model of the rotor with CAD software and prepare it for the 3D printing.
    d. 3D printing of the Savonius rotor by the 3D printer situated in the Fluid Mechanics Department.

e. State of art of techniques or methods used to treat surfaces of 3D printings and make them smoother.
f. Finishing process of rotor surface in order to make the final preparations before experimental tests.

3. Experimental study

   a. Description of the necessary equipment and facilities of the Fluid Mechanics Department laboratory.

      i. Wind tunnel types and characteristics.
      ii. Aerodynamic wind balance features.

   b. Experiment 1: Aerodynamic forces.

      i. Design the fixing system of the Savonius rotor in the wind balance.
      ii. Design the angular positioning system for aerodynamic tests.
      iii. Description of interfaces used in the wind tunnel and wind balance to acquire the results.
      iv. Description of LabVIEW program.
      v. Aerodynamic forces (lift and drag) tests over the Savonius wind turbine.

   c. Experiment 2: Static torque.

      i. Description of the performance of torque sensor.
      ii. Design the support structure and assembling of all components.
      iii. Static torque tests over the Savonius wind turbine.

4. Report

   a. State of the art and development of the project.
   b. Multiple test results comparison.
   c. Summary of budget.
   d. Environmental impact.
   e. Safety and social considerations.
   f. Conclusions and future aspects.

6.2. Scheduling of the project

The scheduling of the project has been made by the free software Gantt Project, which builds a Gantt diagram with relation of tasks along the time since the beginning of the planning.

The scheduling used to organize this project is shown in the Figure 92.

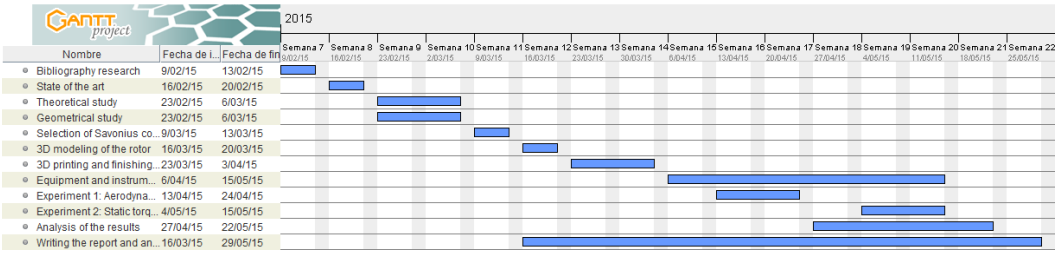

Figure 92 Gantt diagram of the project

Chapter 7

7. Conclusions and recommendations

In general, it is possible to conclude that the experimental study carried out has been developed under expectations. As it is already known, experimental projects are full of unexpected obstacles to face, especially those which has to be done in an academic laboratory where every day there are students and professors using the facilities, such as the present project.

Firstly, the theoretical and geometrical study done at the beginning of this project was essential in order to design the desired model of Savonius wind turbine. Moreover, the 3D printing done to build the rotor was very useful because it saved a lot of time for advancing in other issues, like preparing the necessary material and equipment for experimental testing.

Also, it has been very gratifying to see that the rotor printed has resisted many processes, such as surface treatment or all drillings made on its end plates. This study has proved that printed models can perfectly be used in experimental tests instead of handmade ones.

Then, the previous documentation of facilities and equipment, such as wind tunnel and wind balance, was very useful so as to understand their performance and, in this way, avoid possible errors during tests and data acquisition processes.

One of the main objectives of this project was to compute aerodynamic forces over a Savonius rotor for different phase angles and different wind speeds. This aim has been satisfactorily covered because results obtained showed a huge similarity with the other aerodynamic coefficients computed experimentally, theoretically and numerically. However, some differences were observed with numerical study due to the idealities assumed in CFD simulations.

The second main objective was to compute static torque coefficients produced by the Savonius rotor for different phase angles and for a range of wind speeds. Results obtained were satisfactory too, because they showed a great similarity with numerical and experimental studies. Regarding the ones obtained theoretically, they were not as good due to the ideal hypotheses considered in the approach of the case. After the

analysis of static torque in comparison with the others, it can be concluded that the Savonius rotor designed in this project has better starting torque characteristics than the ones used in the other studies compared. Which is an achievement because one of the aims of this project was to design a more efficient and optimized rotor.

About some recommendations and improvements of this project, firstly, a more accurate theoretical analysis should be made in static torque study in order to obtain results more similar to the experimental ones.

Also, it would be very interesting to calculate the rotating torque of a Savonius rotor to compute the power that can be extracted from it. To do so, it would be needed a good organization of the experiment and an adequate preparation of the necessary equipment, in this way, it would be possible to compute dynamic torque coefficients and power coefficients. With these two parameters it is possible to compare the Savonius rotor in a performance or efficiency scale of wind turbines.

But the rotor not necessarily has to be a Savonius, there are several small scales rotors that can be tested in a wind tunnel, such as a Darrieus rotor for instance.

Finally, one interesting improvement would be to test the additional configurations that have been described in the theoretical and geometrical study at the beginning of this project, in order to check if they really improve the Savonius rotor performance or not.

To sum up, my assessment about this project is that I can say I am very proud of the work done because I have achieved all main objectives of this study. I realized that the experiments carried out are very different from practice sessions done along the degree. They require much more time and much more planning, however, you learn more interesting things because you are working about a topic you have chosen previously, wind turbines in this case. In addition, I have worked in direct contact with the facilities of Fluid Mechanics Department, such as wind tunnel and wind balance, which are nice instruments to work with if you are an aeronautical student.

7.1. Future work

In this section a possible future work must be defined in order to continue the present study or improve it following the recommendations described in the previous section.

Then, the project proposed would be an improved experimental analysis of a Savonius or another small rotor, such a Darrieus wind turbine. As improved it refers to analyze the torque produced by the rotor when rotating, which is an essential parameter to compute the power given by a rotor and, in this way, calculate its performance and efficiency. It would be possible for a future project if the necessary material and instrumentation is prepared adequately.

To do so, state of the art of the rotor selected must be done, because the design of the rotor chosen should be based on previous researches in order to obtain an optimum configuration for experiments. Thus, a great amount of bibliography extracted from scientific databases should be analyzed.

The model tested should be a small scale rotor so as to fit in the test bench of wind tunnel, like the Savonius used in this study. In addition, if it is wanted to build the rotor with a 3D printer, then the model must be done according to size specifications of the printer that will be used. Moreover, it has to be a rotor whose configuration must guarantee the integrity of its structure once printed.

On the other hand, if the rotor is built manually, then only space restrictions of the test bench of wind tunnel must be taken into account.

Finally, as it has been done in this project, the results obtained experimentally should be compared and verified with the ones obtained by a numerical study done with CFD. Both studies should be carried out in parallel and should study the same rotor in the same test conditions in order to get similar results.

7.2. Planning of the future work

The scheduling and task relationship of the future project described in the previous section has been made by the free software Gantt Project as it is shown in the Figure 93. It has been considered that the study is going to be carried out in the spring semester of next year, 2016.

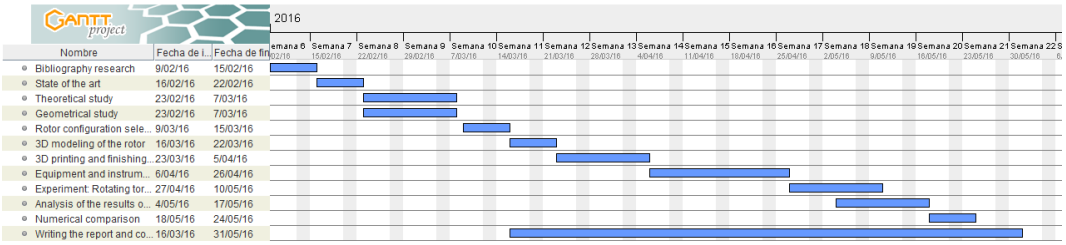

Figure 93 Gantt diagram of the future work

8. Bibliography

[1] P. Jaohindy, S. McTavish, F. Garde, and A. Bastide, “An analysis of the transient forces acting on Savonius rotors with different aspect ratios,” *Renew. Energy*, vol. 55, pp. 286–295, 2013.

[2] “Rotor Savonius,” *Wikipedia*, 2015. [Online]. Available: http://es.wikipedia.org/wiki/Rotor_Savonius. [Accessed: 23-May-2015].

[3] J. L. Menet, “A double-step Savonius rotor for local production of electricity,” *Renew. Energy*, vol. 29, pp. 1843–1862, 2004.

[4] U. K. Saha, S. Thotla, and D. Maity, “Optimum design configuration of Savonius rotor through wind tunnel experiments,” *J. Wind Eng. Ind. Aerodyn.*, vol. 96, pp. 1359–1375, 2008.

[5] N. H. Mahmoud, a. a. El-Haroun, E. Wahba, and M. H. Nasef, “An experimental study on improvement of Savonius rotor performance,” *Alexandria Eng. J.*, vol. 51, no. 1, pp. 19–25, 2012.

[6] K. Irabu and J. N. Roy, “Characteristics of wind power on Savonius rotor using a guide-box tunnel,” *Exp. Therm. Fluid Sci.*, vol. 32, pp. 580–586, 2007.

[7] J. V. Akwa, H. A. Vielmo, and A. P. Petry, “A review on the performance of Savonius wind turbines,” *Renew. Sustain. Energy Rev.*, vol. 16, no. 5, pp. 3054–3064, 2012.

[8] M. H. Nasef, W. A. El-Askary, A. A. AbdEL-hamid, and H. E. Gad, “Evaluation of Savonius rotor performance: Static and dynamic studies,” *J. Wind Eng. Ind. Aerodyn.*, vol. 123, pp. 1–11, 2013.

[9] A. J. Alexander and B. P. Holownia, “Wind tunnel tests on a Savonius rotor,” *J. Ind. Aerodyn.*, vol. 3, pp. 343–351, 1978.

[10] S. Sivasegaram, “Secondary parameters affecting the performance of resistance type vertical-axis wind rotors,” *Wind Eng.*, vol. 2, pp. 49–58, 1978.

[11] F. Mahamarakkalage, “On the Performance and Wake Aerodynamics of the Savonius Wind Turbine,” University of Peradenyia, Srilanka, 1980.

[12] N. J. Roth, "Prototype Design and Performance of Savonius Rotor Based on Irrigation System," University of Britich Columbia, 1982.

[13] V. J. Modi, N. J. Roth, and M. S. Fernando, "Optimum-configuration studies and protoype design of a wind-energy-operated irrigation system," *J. Wind Eng. Ind. Aerodyn.*, vol. 16, pp. 85–96, 1984.

[14] I. Ushiyama and H. Nagai, "Optimum design configuration and performance of Savonius rotors," *Wind Eng.*, vol. 2, pp. 59–75, 1988.

[15] N. Fujisawa, "On the torque mechanism of Savonius rotors," *J. Wind Eng. Ind. Aerodyn.*, vol. 40, pp. 227–292, 1992.

[16] A. Damak, Z. Driss, and M. S. Abid, "Experimental investigation of helical Savonius rotor with a twist of 180°," *Renew. Energy*, vol. 52, pp. 136–142, 2013.

[17] C. Kang, H. Liu, and X. Yang, "Review of fluid dynamics aspects of Savonius-rotor-based vertical-axis wind rotors," *Renew. Sustain. Energy Rev.*, vol. 33, pp. 499–508, 2014.

[18] A. S. Grinspan, U. K. Saha, and P. Mahanta, "Experimental investigation of twisted bladed Savonius wind turbine rotor," *RERIC Int. Energy J.*, vol. 5, no. 1, pp. 1–9, 2004.

[19] U. K. Saha and M. J. Rajkumar, "On the performance analysis of Savonius rotor with twisted blades," *Renew. Energy*, vol. 31, no. 11, pp. 1776–1788, 2006.

[20] M. a. Kamoji, S. B. Kedare, and S. V. Prabhu, "Experimental investigations on single stage modified Savonius rotor," *Appl. Energy*, vol. 86, no. 7–8, pp. 1064–1073, 2009.

[21] B. D. Altan and M. Atilgan, "An experimental and numerical study on the improvement of the performance of Savonius wind rotor," *Energy Convers. Manag.*, vol. 49, no. 12, pp. 3425–3432, 2008.

[22] U. Guide, "HP Designjet 3D Printer HP Designjet Color 3D Printer User Guide." .

[23] U. Guide, "HP Designjet 3D Removal System." .

[24] C. 3D, "ABS vs. PLA," 2014. [Online]. Available: http://www.createc3d.com/abs-vs-pla-que-material-utilizamos/. [Accessed: 14-Apr-2015].

[25] "On 3D printing," *Acetone vapor bath*, 2013. [Online]. Available: http://on3dprinting.com/tag/acetone-vapor-bath/. [Accessed: 15-Apr-2015].

[26] M. A. Díaz Llanos, "Experimental study of the aerodynamic force in a race car," ETSEIAT, 2014.

[27] G. Raush, R. Castilla, P. J. Gamez-Montero, J. Wojciechowski, and E. Codina, "Flexible rod design for educational wind balance," *Exp. Tech.*, pp. 1–9, 2013.

[28] M. A. Díaz Llanos, "Experimental study of the aerodynamic force in a race car - ANNEX II - Calibration Process," 2014.

[29] Ohara et al., "Turbo machinery," *Annu. reports 13*, vol. 56, 1983.

[30] R. Castilla, P. J. Gámez, M. Garcia, and G. Raush, "Fluid Mechanics Laboratory for degree in Aerospace Technology and degree in Aerospace Vehicles," Terrassa, 2012.

[31] N. Sinaga, "Mekanika Fluida II," 2013. [Online]. Available: http://slideplayer.com/slide/252881/#. [Accessed: 05-May-2015].

[32] K. Irabu and J. N. Roy, "Study of direct force measurement and characteristics on blades of Savonius rotor at static state," *Exp. Therm. Fluid Sci.*, vol. 35, no. 4, pp. 653–659, 2011.

[33] P. A. Martorell, "Numerical study of flow through a Savonius wind turbine," ETSEIAT (UPC), 2015.

[34] "Aerodynamic for students," *Univeristy of Sydney*, 2005. [Online]. Available: http://www-mdp.eng.cam.ac.uk/web/library/enginfo/aerothermal_dvd_only/aero/fprops/introvisc/node11.html. [Accessed: 25-May-2015].